Diel vertical migration and frontal variability of acoustic backscatter in the Balearic Sea

by

Helena R. Cheslack

B.S., United States Naval Academy (2016)

Submitted to the Department of Earth, Atmospheric and Planetary Sciences
in partial fulfillment of the requirements for the degree of

Master of Science in Physical Oceanography

at the

MASSACHUSETTS INSTITUTE OF TECHNOLOGY

and the

WOODS HOLE OCEANOGRAPHIC INSTITUTION

September 2023

Author . . . . . .
Joint Program in Oceanography/Applied Ocean Science and Engineering
Massachusetts Institute of Technology
& Woods Hole Oceanographic Institution
August 11, 2023

Certified by . . . . . .
Dr. Amala Mahadevan
Thesis Supervisor
Woods Hole Oceanographic Institution

Accepted by . . . . . .
Dr. Amala Mahadevan
Chair, Joint Committee for Physical Oceanography
Massachusetts Institute of Technology
& Woods Hole Oceanographic Institution

Diel vertical migration and frontal variability of acoustic backscatter in the Balearic Sea

by

Helena R. Cheslack

Submitted to the Department of Earth, Atmospheric and Planetary Sciences
Massachusetts Institute of Technology & Woods Hole Oceanographic Institution
on August 11, 2023, in partial fulfillment of the
requirements for the degree of
Master of Science in Physical Oceanography

Abstract

Acoustic Doppler current profilers (ADCPs) use active sonar to measure current velocities by measuring the sound returned by scatterers (most often zooplankton) in the water column. The volume of scatterers, or echo intensity, has been used to measure the abundance of zooplankton and characterize diel vertical migration (DVM). DVM is the mass vertical movement of zooplankton and fish between the surface waters where they feed at night, and the mesopelagic zone where they avoid predators during the day; it is considered the largest migration of biomass on Earth, happens in every ocean, and is important to the global carbon cycle.

This thesis uses a combination of data that I helped acquire during the Office of Naval Research-funded CALYPSO 2022 field campaign in the Balearic Sea. Acoustic backscatter from a 38kHz ADCP and a 150kHz ADCP is translated into mean volume backscattering strength (MVBS) to characterize the sound scattering layers (SSLs) in the Balearic Sea. WireWalker data is used to model subsurface light. The MVBS is compared to measurements of temperature, salinity, chlorophyll concentration, and dissolved oxygen (DO) from the EcoCTD, a towed instrument that simultaneously measures hydrographic and biological parameters. The analysis reveals one permanent scattering layer at 300m – 600m and two migrating scattering layers in the top 50m and between 100m – 300m. The layers are likely made up of zooplankton like krill and pteropods and pelagic fish. The speed of vertical migration ranges from 1 – 11cms^{-1}, and migrators are follow isolumes during migration times. DVM has the strongest effect on backscatter anomalies, but during daytime and nighttime, DO is most correlated with the backscatter anomaly.

We demonstrate that ADCPS can be used to characterize SSLs and DVM. The uniquely co-located EcoCTD data from CALYPSO enables us to compare the frontal variability in scatterers to variability in biological and physical parameters. Characterizing the SSLs, DVM, and frontal variability of acoustic backscatter furthers understanding of the global carbon cycle.

Thesis Supervisor: Dr. Amala Mahadevan
Title: Senior Scientist
Woods Hole Oceanographic Institution

Acknowledgments

The land on which this thesis was written is the traditional unceded territory of the Wôpanâak (Wampanoag) peoples. We recognize the perpetuated detrimental effects that systemic governmental oppressions have had on indigenous communities as a result of colonization. We honor and respect the many diverse indigenous people connected from time immemorial to this land. I am personally grateful for the lectures, discussions, and resources that I have had access to through Woods Hole Oceanographic Institution to better understand indigenous science.

Thank you to the United States Navy for funding my graduate education at the Massachusetts Institute of Technology and Woods Hole Oceanographic Institution (MIT-WHOI) Joint Program. I am grateful that I had the past two years to focus solely on my classwork and research that has culminated in this thesis. I worked tirelessly in my first five years as a Naval officer to achieve my dream of coming to the MIT-WHOI Joint Program which I set my sights on as a Midshipman at the Naval Academy. I am beyond honored and grateful to have been selected by the Navy to represent the Meteorology and Oceanography (METOC) community at MIT and WHOI over the past 27 months. This opportunity is unmatched and has truly provided more exposure, self-discovery, challenges, and life-long connections than I ever could have imagined.

I would like to thank my advisor, Amala Mahadevan, who welcomed me into her lab and has included me in every possible way. Her mentorship, guidance, brilliance, and encouragement to try the things that interest me have had an indelible effect on my personal and professional development. I would like to thank Kenneth Foote whose acoustics course and mentorship helped shape the fundamental understanding for this thesis. I would also like to thank Andrey Shcherbina whose guidance and mentorship were essential for the basis of this work.

I am thrilled to have been a member of the Mahadevan Lab throughout my time here. From weekly group meetings to winter hiking on our lab retreat, I could not have asked for a better group. Thank you to Alex Kinsella, Leo Middleton, Jing He, Roger Wu, and Katy Abbott for the camaraderie, scientific discussions, and friendship. Thank you to Alex Kinsella and Leo Middleton for the discussions and MATLAB help during my research.

I do not know how I would have gotten through the first semester of classes without the other members of my cohort: Margaret Gregory, Brynn Hamilton, Elena Perez, Anthony Meza, and Oaklin Keefe. I certainly got the challenge I asked for, luckily I had the most amazing friends and classmates to go through it with. The broader Joint Program student community has been incredible. I have never felt so welcomed and included as I have here. Thank you to all of the Joint Program students for fostering such a welcoming environment.

I helped collect the data for this cruise on the *N/O Pourquoi Pas?* during the 2022 CALYPSO field campaign. This was my first oceanographic research cruise and I'm glad to have bonded with the members of my lab group who were also at sea: Katy, Leo, Alex, and Roger. I stood an 8-hour night watch with Alex and Drew Cole, one of the technicians who led our watch skillfully. Thank you to the scientific

party, headed by Amala and Eric D'Asaro, for an exciting research cruise, and to the crew of the *N/O Pourquoi Pas?* who tolerated our presence on the Bridge and kept us safe.

Most importantly, I'd like to thank my family. First, thank you to my husband, Nighel Cobb. I am grateful for your unwavering support and for your encouragement to take all of the opportunities I could, even if it meant more time away from home. Thank you to my parents, Randy Kurtz and Brian Cheslack, who are always the most supportive of anything I do and both spent time editing this thesis. Thank you to my wonderful siblings Vivian and Kai who I am grateful to have seen more over the past two years.

Support for the research in this thesis was funded by the U.S. Navy's Civilian Institution (CIVINS) Office with the MIT-WHOI Joint Program, the WHOI Academic Programs Office, and the Office of Naval Research CALYPSO DRI grant N00014-21-1-2702.

Contents

List of Figures

List of Tables

Chapter 1

Introduction

1.1 Motivation

Zooplankton are present in all the world's oceans and represent an extensive array of diversity in taxonomy and range in size from a few micrometers to several meters. Zooplankton and pelagic fish represent a major link between primary producers and higher trophic levels in pelagic food webs, which is central to regulating the exchange of CO_2 between the atmosphere and the surface ocean (Steinberg & Landry, 2017). Within the food web, zooplankton serve as both primary consumers and recyclers that transform particulate carbon and nutrients. The estimated global zooplankton biomass in the top 500m of the ocean is 0.403 PgC (Petagram of Carbon, where 1PgC = 1 gigaton of Carbon). Zooplankton are essential to the biological carbon pump which is the suite of biological processes that mediate the transport of carbon from the upper ocean to depth. The ways in which zooplankton cycle carbon include respiration, excretion, sinking of carcasses of dead zooplankton, and diel vertical migration (DVM).

DVM is the mass vertical movement of zooplankton and pelagic fish across the world's oceans between surface waters and the mesopelagic zone. It is thought to be the largest migration of biomass on the planet and it happens every single day in all the world's oceans (Brierley, 2014). The most common type of DVM is noctur-

nal DVM, where organisms feed in the surface waters during the day and swim to deeper waters to avoid predation at night. DVM is a major zooplankton-mediated carbon export pathway (Figure 2-1) (Steinberg & Landry, 2017). DVM is an important phenomenon to characterize, especially as we seek to better understand the effects of our changing climate.

The organisms that practice DVM make up sound scattering layers (SSLs) in the oceans which are detectable as acoustic backscatter. Acoustic backscatter can be measured by acoustic instruments such sonar, echosounders, and acoustic Doppler current profilers (ADCPs). SSLs can be made up of organisms that practice DVM, referred to as migrating scattering layers in this thesis, or they can be relatively stationary in the water column and are referred to as permanent scattering layers. SSLs are so distinct in acoustic backscatter that they were initially thought to be the ocean bottom when they were discovered by US Navy sonar in the 1940s. The characterization and understanding of SSLs regionally and seasonally is important for operational sonar use, particularly for the safety of navigation of the US Navy submarine fleet. ADCPs are ubiquitous on oceanographic research vessels and collect acoustic backscatter as a byproduct of calculating current velocities.

The CALYPSO 2022 Field Campaign successfully collected a large and unique data set of both physical and biological measurements in the Balearic Sea located in the Western Mediterranean. Using this data set, the work in this thesis addresses the following questions:

- What is the distribution and strength of SSLs in the Balearic Sea? Is DVM detected by the acoustic backscatter? How fast are migrators swimming?

- How does acoustic backscatter from ADCPs compare to biological and physical parameters like temperature, salinity, dissolved oxygen, and chlorophyll concentration? Which parameter or parameters control the frontal variability of acoustic backscatter?

1.2 Background

1.2.1 CALYPSO Research Initiative

This work uses data from the "CALYPSO" (Coherent Lagrangian Pathways from the Surface Ocean to Interior) program, an Office of Naval Research (ONR) Departmental Research Initiative. The goal of CALYPSO is to observe, understand, and predict the three-dimensional pathways by which water from the surface ocean makes its way to the interior. CALYPSO involved innovative observational techniques along with process study models, predictive models, and data synthesis to diagnose and predict the physical processes that underlie subduction and transport across the base of the surface mixed layer (Mahadevan et al., 2020). CALYPSO focuses on the submesoscale to understand vertical transport.

Submesoscale refers to processes that take place on lateral scales of kilometers to tens of kilometers and are characterized by a Rossby number, $Ro = \varsigma/f$, and Richardson number, $Ri = N/U_z$, of $\mathcal{O}(1)$. Processes at the submesoscale are not in geostrophic balance, enabling the intensification of the vertical component of velocity. Understanding vertical velocities at the submesoscale is critical for understanding the carbon cycle, biogeochemical processes, and the transfer of energy from large (meso-)scales to small scales (Mahadevan et al., 2020).

Since density surfaces at fronts are steeply sloping, there will be a vertical component of along-isopycnal motion that generates subduction (Freilich & Mahadevan, 2019). Subduction is the transport of water from the surface mixed layer into the stratified pycnocline; the pycnocline is the layer where the vertical density gradient is the greatest in the water column. Subduction can occur through the seasonal transformation of the mixed layer and the large-scale circulation through diabatic processes, or it can occur along sloping isopycnals at fronts due to submesoscale processes (Freilich & Mahadevan, 2021). CALYPSO encompassed three field campaigns in the Western Mediterranean Sea in 2018, 2019, and 2022. This work utilizes data from the 2022 field campaign.

CALYPSO 2022 Field Campaign

The 2022 CALYPSO field campaign was a 23-day long research cruise that departed from Toulon, France, and took place in the Balearic Sea in the Western Mediterranean Sea. It involved two oceanographic research vessels, the French *N/O Pourquoi Pas?*, and the Dutch *R/V Pelagia*. I had the opportunity to embark on my first oceanographic research cruise on the *N/O Pourquoi Pas?* as part of the 30+ scientific crew. Some of the data I helped to collect is used in this thesis.

Figure 1-1: Photo of the *R/V Pourquoi Pas?* in Toulon, France prior to the CALYPSO cruise in February-March 2022.

The *N/O Pourquoi Pas?* is the flagship of IFREMER (in English, "French Research Institute for Exploitation of the Sea"), France's national marine science research institute. We used an adaptive sampling method with numerous instruments to collect physical and biological data to further the goal of CALYPSO. The scientific party, led by Senior Scientists Dr. Amala Mahadevan (WHOI) and Dr. Eric D'Asaro (University of Washington), devised a plan of the watch each day and night to best accomplish the scientific goals of CALYPSO by sampling the constantly evolving submesoscale features. For example, if we saw an interesting submesoscale eddy to the south that the scientists agreed would be of interest to sample, we would steam to the south. Many of these adaptive sampling decisions were possible because of in-situ data I helped to collect every day, as well as remote sensing and modeling tools.

The instruments onboard the *N/O Pourquoi Pas?* included the CTD (conductivity, temperature, and depth) rosette, the EcoCTD (see section 1.5.1), the MVP (see section 1.5.2), WireWalkers (see section 1.5.3), three shipboard mounted ADCPs (see section 1.3), and over 300 drifters. I stood an eight-hour night EcoCTD watch with Dr. Alex Kinsella (WHOI) and oceanographic technician, Drew Cole. We took turns manually letting out and reeling in the EcoCTD at the stern of the ship for hundreds of individual EcoCTD profiles. I also assisted PhD candidate, Kathleen Abbott, in collecting dozens of water samples during CTD casts for her respiration experiments.

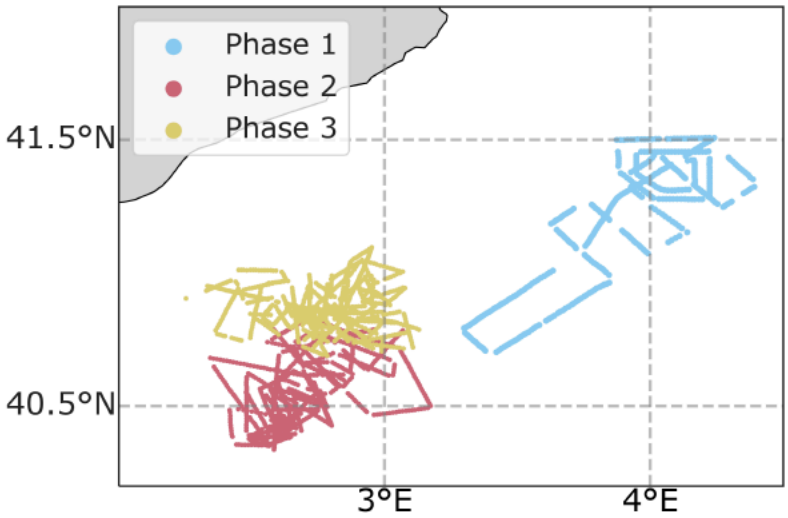

Figure 1-2: Map of all EcoCTD profiles during the CALYPSO 2022 cruise with the three phases of the cruise separated into blue, red, and yellow. Figure courtesy of Kathleen Abbott.

The 2022 field campaign can be divided into three distinct phases (Figure 1-2) as a result of this adaptive sampling. We started Phase 1 in the Gulf of Lion, where strong surface cooling and evaporation from the mistral winds generate open ocean deep convection (Goffredo & Dubinsky, 2013). We then steamed southeast to sample a high-chlorophyll cyclonic eddy as it elongated into a ridge and collapsed into two smaller eddies during Phase 2, and for Phase 3 we sampled another cyclonic eddy to the north as it entrained a filament of colder water.

1.2.2 Region of Study

The Mediterranean Sea is a semi-enclosed evaporation basin that is connected to the Atlantic Ocean by the Strait of Gibraltar, and to the Black Sea by the Dardanelles/Marmara Sea/Bosphorus system. The Mediterranean is composed of two sub-basins, western and eastern, with distinct characteristics that are connected by the Sicily Strait (Goffredo & Dubinsky, 2013). The Mediterranean is an extremely important body of water for biodiversity, food, and recreation and profoundly impacts the human health and well-being of the countries that border it. Due to its unique hydrographic characteristics, it is considered a “miniature ocean” or “laboratory basin” by some scientists who have pointed out that the same oceanographic processes that occur in the Mediterranean Sea are happening in all the world’s oceans. In the Mediterranean, these processes such as water mass formation, eddies, frontal activities, and subduction are occurring on a shorter time scale. This is especially relevant under increased climate stressors, as the climate and anthropogenic impacts being seen in the Mediterranean Sea will likely be seen globally (Schroeder & Chiggiato, 2022).

The western Mediterranean Sea is an ideal location for studying submesoscale processes. The 2018 and 2019 CALYPSO field campaigns took place in the Alborán Sea, which is bordered by Spain to the north and Morocco and Algeria to the south. Fresher Atlantic ocean water flows through the Strait of Gibraltar and meets saltier Mediterranean water to form an unstable front (Mahadevan et al., 2020). The CALYPSO 2022 field campaign took place in the Balearic Sea which is to the north of the Alborán, located between the Balearic islands, the Spanish mainland, and the Gulf of Lion in the western Mediterranean. Figure 1-3 is a map of the Balearic Sea with bottom topography; the blue line indicates the extent of the Balearic Sea.

The Balearic Sea is considered a transition basin between the cold, saline water in the Gulf of Lion and the warmer, less saline water in the Alborán Basin. The cold, fresh Atlantic Water (AW) that flows through the Strait of Gibraltar meets the saltier and more dense Mediterranean water in the Alborán Basin where it is modified

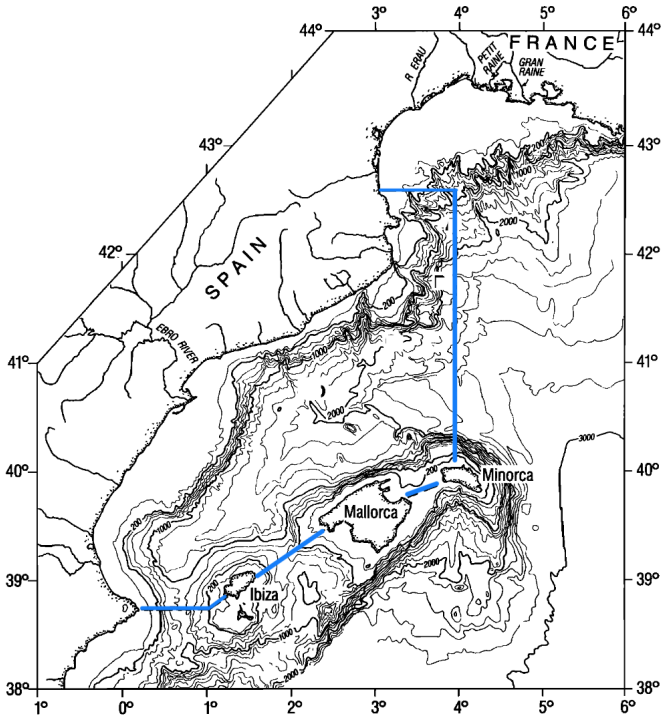

Figure 1-3: A map of the Balearic Sea location (outlined in blue) and bottom topography. Reprinted from Garcia et al., 1994.

through strong evaporative fluxes to produce warmer and saltier Modified Atlantic Water (MAW). The water in the Balearic Sea contains the colder and saltier MAW, with its circulation controlled by atmospheric forcing.

The main currents depicted in Figure 1-4 are the Northern Current and the Balearic Current. The Northern Current is formed by the Atlantic water flow from the Balearic basin joining that from the Tyrrhenian Sea. The Northern Current follows the continental slope from the Ligurian Sea to the Catalan Sea and the Balearic Current branches off in the Balearic subbasin. The Atlantic water that flows across the Balearic channels forms the Balearic Current which follows the northern side of the Balearic Islands and displays high variability, mainly driven by fluctuations in the input from the Algerian Basin. A surface front to a depth of about 200m is associated with the Balearic Current and separates the recent Atlantic water of the current from the resident waters of the northern basin (Goffredo & Dubinsky, 2013).

The Balearic also has significant mesoscale variability which is associated with

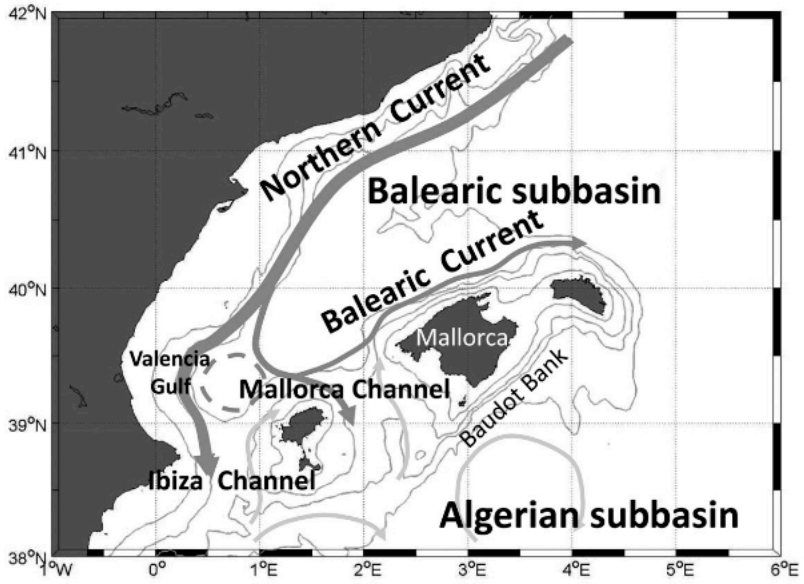

Figure 1-4: The Balearic Sea (subbasin) and the main currents that characterize the regional circulation. The Northern and Balearic currents are represented as gray arrows, and the Algerian gyres are represented as light gray arrows. Isobaths are represented by light gray lines. Reproduced from Peña et al., 2014.

two thermohaline fronts on both sides of the basin. These fronts are characterized by instabilities such as mesoscale eddies, filaments, and mid-depth intrusions (Garcia et al., 1994). The filaments, mid-depth intrusions, and frontal slopes in this region are ideal for studying submesoscale processes.

Water Masses

The water masses important to understanding the region of study include the MAW found in the Balearic, the Levantine Intermediate Water (LIW), and the Western Mediterranean Deep Water (WMDW). The LIW is formed through excessive heat loss and evaporation in the northeastern Levantine basin in the eastern Mediterranean. It then spreads at intermediate depths (300 – 800m) through the whole basin to exit through the bottom layer of the Gibraltar Strait into the Atlantic Ocean.

Each subbasin in the Mediterranean contains a closed thermohaline cell that drives Deep Water Formation (DWF). In the Western Mediterranean, the WMDW is formed in the cyclonic gyre of the Gulf of Lion. The Gulf of Lion is exposed to the

Mistral and Tramontane which are periodic wind events caused by northerly winds being channeled and intensified by the continental orography. These winds are associated with cold and dry polar air masses in the winter; this cold dry air over seawater causes the sea surface to undergo strong cooling through evaporation, increasing the water density. This produces convective mixing between the surface layer and deeper layers. The erosion of the stratification of the surface by winter storms is the critical point for deep convection (Schroeder & Chiggiato, 2022). The dynamics of water masses in the Mediterranean are also highly sensitive to climate and anthropogenic changes and can be affected by variations in river freshwater discharge and other factors (Goffredo & Dubinsky, 2013).

Dissolved Oxygen

Dissolved oxygen (DO) is the concentration of oxygen in seawater [μmolkg^{-1}] and depends on temperature since solubility decreases with increasing temperature. The DO distribution in the Mediterranean Sea has been studied in detail, and convection cells provide an important mechanism for ventilation in the Mediterranean. The levels of DO concentrations in the Mediterranean are very sensitive to the effects of global warming, and a global decrease in oxygen is predicted by climate and biogeochemical models (Schroeder & Chiggiato, 2022). DO is often associated with specific water masses; it is a proxy for the physical and biological processes that the water masses undergo. Outside of the deep convection zone in the Western Mediterranean, the LIW has a stronger minimum of DO. In the WMDW, the DO concentrations are higher than in intermediate layers because of the ventilation of deep water that occurs in the Gulf of Lion due to deep convection.

Zooplankton and Micronekton

The study of zooplankton in the Mediterranean Sea dates back nearly 200 years, and the information about species variability and their behavior is rich. However, it is mostly limited to coastal studies (Goffredo & Dubinsky, 2013). According to a 2007

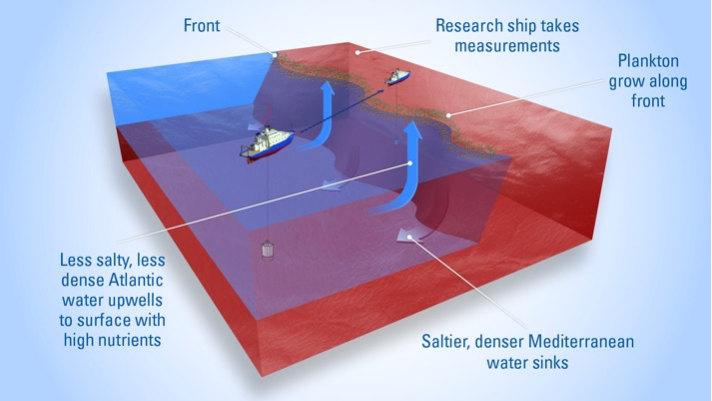

Figure 1-5: Schematic illustration of a front. A front is the confluence of two distinct water masses, they are indicated by distinct colors. In this case fresher, lighter Atlantic water meets saltier, denser Mediterranean water. As the front meanders and creates instabilities, upwelling and downwelling is generated as indicated by the arrows. The CALYPSO ONR Departmental Research Initiative sought to study the dynamics at these fronts, where there is also usually an abundance of plankton. Reproduced from Freilich, 2018.

study focused on the Mallorca channel, the most abundant species of zooplankton in the Balearic Sea is copepods with over 50% of the total biomass. Other important groups include gelatinous plankton, salps, and pteropods (Fernández de Puelles et al., 2007). The literature generally points to peaks of zooplankton abundance two to three times a year based on seasonality and phytoplankton blooms. In the Mallorca channel, the standing stocks of zooplankton appear to be highest in late winter – spring, which is when the 2022 CALYPSO research cruise took place (Fernández de Puelles et al., 2004).

There have been several studies in the western Mediterranean about the impact of mesoscale structures like density fronts on the distribution and diversity of zooplankton. The Balearic Current has been shown to be a transitional zone with overall higher biological production due to high phytoplankton biomass and primary production; this also includes higher biomass of zooplankton (Goffredo & Dubinsky, 2013). In fact, these fronts such as the one formed by the Balearic current are exactly what the CALYPSO research initiative sought to study. This idea is depicted in the graphic in Figure 1-5. Density fronts in the northwestern Mediterranean have been shown to have differing effects on different species of zooplankton. Larger copepod species and krill larvae have been shown to be highly abundant along

the front while salp and smaller copepods did not have a distinct pattern (Molinero et al., 2008).

Mesopelagic fish are part of the category of micronekton which are small (2 – 20cm) organisms that also include crustaceans, cnidarians, and mollusks. These organisms often occupy the shallow part of the water column and are important for the global carbon cycle. A 2014 study used acoustics and net tows to study the abundance, species composition, and migration patterns of mesopelagic fish near the Balearic Islands. They found the most abundant fish to be the bristlemouth (*Cyclothone braueri*) and the hatchetfish (*Argyropelecus hemigymnus*). These species conduct daily vertical migrations which will be discussed at length in Chapter 2 (Peña et al., 2014).

1.3 Acoustic Doppler Current Profilers (ADCPs)

A concerted effort to develop current measuring devices using Doppler shift began in the 1960s and the technology has continued to advance with numerous applications since (Woodward & Appell, 1986). ADCPs were first introduced in the late 1970s as an adaptation to the Doppler speed log, which is an instrument that measures the speed of ships through the water or over the seafloor (Gordon & Instruments, 2011). ADCPs are primarily used to measure horizontal and vertical currents by measuring the Doppler shift of “passive” particles in the water column. They are mounted on most oceanographic research vessels and are primarily used for physical oceanography, but have biological oceanography applications as well.

The first commercially available ADCPs in the 1980s used a narrowband, single-pulse autocorrelation method – a mathematical method useful for comparing echoes – to compute the Doppler frequency spectrum. Beginning in 1991, the main ADCP production company, RD Instruments, introduced a broader bandwidth ADCP. These so-called broadband ADCPs were meant to greatly increase the information returned by the ADCP and are now the prevailing ADCP type (Wilson et al., 1997).

1.3.1 The Physics behind ADCPs

ADCPs are made up of multiple (usually three or four) transducers which are able to convert sound to electricity and vice versa. The active elements in the transducers are piezoelectric ceramic disks that expand or contract under the influence of an electric field. Piezoelectric refers to the material in the transducer that has the capacity to generate electrical current when exposed to mechanical stress or vibration (Urick, 1983). Different types of ADCPs (hull-mounted, moored, bottom-mounted) may have different transducer configurations based on the purpose.

ADCPs work by active sonar; they use sound to measure current velocities by actively transmitting sound pulses at a certain frequency and measuring the frequency shift (Doppler) of the returning sound as it is scattered by the particles in the water. The Doppler effect is defined as a change in the observed sound pitch that results from relative motion. A common example is the difference in pitch of an ambulance siren as it approaches you, versus, as it drives away from you. The pitch will be higher as it approaches and lower as it recedes and this change in pitch is directly proportional to how fast the ambulance is moving.

ADCPs use the Doppler effect to measure current velocities by transmitting sound pulses at a fixed frequency and recording the echoes returned from sound scatterers in the water (Gordon & Instruments, 2011). Due to the Doppler shift, scatterers in the water column moving away from the ADCP will have a lower frequency when returned to the ADCP, and scatterers moving toward the ADCP will have a higher frequency. ADCPs rely on these scatterers in the water to calculate current velocities (Flagg & Smith, 1989). A key assumption for the use of ADCPs is that on average the scatterers move at the same horizontal velocity as the water. The primary scatterers of acoustic energy are zooplankton, with sizes on the order of one-millimeter (Flagg & Smith, 1989; Gordon & Instruments, 2011; Plueddemann & Pinkel, 1989).

Typical scatterers in most of the world's oceans, including the Mediterranean Sea, are zooplankton such as copepods, pteropods, and euphausiids which are

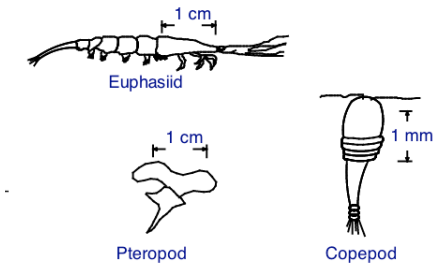

Figure 1-6: Typical ocean scatterers. Reproduced from (Gordon & Instruments, 2011).

depicted in Figure 1-6. ADCPs can also reflect off other scatterers including suspended sediment, detritus, and density gradients. The transmitted sound from the ADCP pulse scatters in all directions from the scatterers, reflecting a small amount of sound back to the ADCP. This sound is Doppler shifted and is referred to as backscatter. The concentration of scatterers affects the range of the ADCP because the presence of more scatterers means more sound will be reflected back to the ADCP.

Each ADCP in this study has four transducers that are offset from the instrument at a certain angle and each produces a beam (see Table 1.1). The multiple beams are necessary to measure each velocity component (for example, north and east components), and having four beams allows for estimates of two horizontal velocity components and two estimates of vertical velocity (Gordon & Instruments, 2011). ADCPs come in a range of frequencies. In general, high-frequency ADCPs (300 kHz) provide high-resolution data close to the surface, while low-frequency (38 kHz) ADCPs provide low-resolution data but can profile to greater depths.

Broadband Doppler Processing

Broadband technology enables ADCPs to take advantage of the full signal bandwidth available for measuring velocity by transmitting coded pulses within a single pulse that makes multiple measurements. An autocorrelation method is used but, rather than a single pulse as in the narrowband method, the broadband ADCPs calculate the phase difference between the coded pulses. The coded pulses are trans-

mitted inside a single long pulse, which allows the ADCP to obtain many echoes from many scatterers. This allows the ADCPs access to much more information than narrowband ADCPs to estimate velocity, typically reaching 100 times more bandwidth. This means that the autocorrelation method is more complex than the one used for narrowband ADCPs. The specific method is described in more detail in the useful and comprehensible RD Teledyne Instruments ADCP Primer (Gordon & Instruments, 2011).

Data Output

The ADCPs output four different types of data: velocity, echo intensity, correlation, and percent good. The velocity data includes horizontal and vertical velocities with units of mm s^{-1}. Echo intensity is obtained from the receiver's received signal strength indicator (RSSI) circuit and is output in counts. Correlation and percent-good data are measures of data quality. During the CALYPSO cruise, the current velocity data was used to better diagnose the location of fronts and other submesoscale features. This thesis focuses on the echo intensity data which is often considered a byproduct of ADCP data, while velocity is the sought after data in physical oceanography.

1.3.2 ADCPs Onboard the *N/O Pourquoi Pas?*

The *N/O Pourquoi Pas?* had three broadband, mounted shipboard ADCPs during the 2022 CALYPSO field campaign: a 38kHz Teledyne Ocean Surveyor; a 150kHz Teledyne Ocean Surveyor; and a 300kHz Teledyne Workhorse Monitor. The 38kHz and 150kHz ADCPs were already mounted on the *N/O Pourquoi Pas?* and maintenance and data collection were managed by the crew. Data was collected for the entire cruise length from February, 18 to March, 11, 2022. The 300kHz ADCP was mounted specifically for the CALYPSO cruise to try to measure current velocities in the top 25 meters of the water column since the high-frequency ADCPs have higher resolution near the surface. Table 1.1 lists relevant technical specifications

of the shipboard-mounted ADCPs used in this work.

Specifications	38 kHz	150 kHz	300 kHz
Type of ADCP	Ocean Surveyor	Ocean Surveyor	Workhorse Monitor
Max Profiling Range	1000m	400m	154m
Ping Rate	0.4 Hz	1.5 Hz	2 Hz
Beam Angle	30°	30°	20°
Dynamic Range	80 dB	80 dB	80 dB

Table 1.1: Relevant specifications for the three shipboard ADCPs onboard the *N/O Pourquoi Pas?* during the 2022 CALYPSO field campaign.

The ADCP data was quality controlled after the cruise for several parameters pertaining to the current velocity calculations. However, since this work is focused on the relative backscatter concentration, the raw echo intensity measurements were used in the data analysis described in sections 2.3 and 3.1.

1.4 ADCP Backscatter

1.4.1 Echo Intensity

Since ADCPs rely on acoustic energy to measure current, they simultaneously measure physical and biological parameters. In order to calculate current velocities using the Doppler effect, ADCPs must measure the concentration of scatterers in the water column which are most often zooplankton. This measurement is called echo intensity in the RD Instruments manual and in the raw data files (Gordon & Instruments, 2011). The data analyzed for this study was the intensity of the backscattered acoustic signal rather than its Doppler shift.

The echo intensity in counts is a relative measurement of the presence of scatterers in the water column and has been recognized as a potential tool for understanding zooplankton abundance since the 1980s. The echo intensity measurement is dependent on the acoustic frequency of the ADCP due to the ratio of the wavelength and the size of the scatterers (Deines, 1999). The three ADCPs with different frequencies (38kHz, 150kHz, and 300kHz) onboard the *N/O Pourquoi Pas?*

would therefore detect different-sized scatterers. The echo intensity or amplitudes from the raw ADCP data were used to analyze the sound scattering layers, vertical migration patterns, and frontal variability. It is important to note that the ADCPs used in this study are not calibrated for absolute backscatter measurements, but the echo intensity measurements are still useful for relative measurements.

Echo intensity depends on sound absorption, beam spreading, transmitted power of the transducer, and the backscatter coefficient. The approximate equation for echo intensity from the Teledyne Instruments ADCP Primer is:

$$EI = SL + SV + C - 20log(R) - 2\alpha R. \tag{1.1}$$

The EI is echo intensity in decibels (dB), SL is transmitted power or source level in dB, α is the absorption coefficient in dBm^{-1} (explained in more detail in Chapter 2), and R is the distance from the transducer to the depth cell in meters. There is an included constant, C because the measurement is relative rather than absolute (Gordon & Instruments, 2011).

Much of the data analysis in Chapters 2 and 3 is reported in decibels. Decibels (dB) is a unit that measures the intensity of sound by comparing it with a given reference intensity on a logarithmic scale. The reference intensity of underwater sound is the intensity of a plane wave with an rms pressure equal to 1 micropascal (μPa). The decibel is a convenient relative unit that allows for easy comparison of large changes of variables and permits simpler math in understanding underwater acoustics (Urick, 1983).

1.4.2 Target Strength

Target strength refers to the echo returned by an underwater target. The target can be of military interest like ships, submarines, or mines, or biological organisms like fish or zooplankton (Urick, 1983). The target strength of zooplankton depends on the characteristics of the individual organisms. Such characteristics might include whether the zooplankton are gelatinous or hard-shelled, what shape they

are, whether or not they have gas-inclusions, and what stage of development they are in. These all vary greatly and are difficult to quantify, especially for such small organisms. Even more complex is that the swimming orientation of the zooplankton can affect the acoustic signal. Even though the ADCP echo intensity is a measurement of the relative backscatter, the characteristics and swimming orientation of the zooplankton can still affect the backscatter signal. For example, the swimming behavior may be different for zooplankton swimming toward the surface versus to depth due to the added help from gravity (Tarling et al., 2001).

1.4.3 Frequency Dependence

The wavelength for various ADCP frequencies can be calculated using the following relationship where the speed of sound in seawater is c = 1500 ms^{-1}, f is the ADCP frequency and λ is the wavelength:

$$c = f\lambda. \tag{1.2}$$

ADCP Frequency	Wavelength	Organism Size	Smallest Organisms
300 kHz	5mm	1.25 – 2.5mm	zooplankton (copepods)
150 kHz	1cm	2.5 – 5mm	zooplankton (krill and pteropods)
38 kHz	4cm	1 – 2cm	macrozooplankton and micronekton (pteropods and pelagic fish)

Table 1.2: Wavelength and expected detectable organism size for the three ADCPs mounted on the *N/O Pourquoi Pas?*.

Table 1.2 indicates the expected minimum size of detected organisms for each ADCP frequency used in this study. The three frequencies are expected to detect different-sized organisms. The 300kHz has the highest resolution and is therefore expected to detect the smallest organisms; in the Balearic Sea the 1 – 2mm ex-

pected organisms would be zooplankton such as copepods which are prevalent in every ocean. The high resolution of 300kHz is limited to the upper ocean. In this case, the 300kHz ADCP only reached 140m making it difficult to use for the analysis in this work. The 150kHz ADCP measured to about 400m and is expected to detect zooplankton such as krill (1 – 2cm) and pteropods (2 – 8mm) in the Balearic Sea. Previous studies in the Western Mediterranean Sea have calibrated ADCPs in the 150kHz range with net tows and found that Northern krill (*Maganyctiphanes norvegica*) and the pteropod *Cavolinia inflexa* are prevalent and detectable in this region (Tarling et al., 2001). While the 38kHz data has the lowest resolution, it also probes the deepest, up to 800m during CALYPSO. The 38kHz ADCP backscatter would be expected to detect macrozooplankton and micronekton which range in size from 2 – 20 cm. This includes krill at 1 – 2cm and other organisms such as mollusks, jellyfish, and pelagic fishes. There are several pelagic fish species in this region that are known to practice diel migration patterns and have been characterized using echosounder data (Peña et al., 2014).

1.4.4 Measurement of Zooplankton

In the decades following the development of ADCPs to measure the velocity of ocean currents, scientists have developed uses for the ADCP byproduct of echo intensity. Pioneering work in the 1980s – 1990s used ADCPs to calibrate backscatter with zooplankton abundance and characterize diel migration patterns (Flagg & Smith, 1989; Heywood et al., 1991; Plueddemann & Pinkel, 1989). In the field of bioacoustics, researchers generally use echosounders to detect and quantify organisms in the water column. Echosounders also use active sonar like ADCPs but are specifically built and calibrated for detecting organisms. Researchers model the types of organism to quantify the abundance and distribution of commercially important fish stocks, micronekton, and zooplankton.

Early Studies

Pluedemann and Pinkel (1989) used a narrowband 67kHz ADCP to characterize sound scattering layers (SSLs) in the eastern North Pacific Ocean, where previous characterization of SSLs had been carried out using low frequency (1 – 20kHz) echosounders. The 67kHz ADCP was able to measure as deep as 1200m whereas previous studies had been limited to the top 300m. Additionally, the ADCP ran continuously during the 13-day study, making it possible to look more closely at the SSL changes from day to day. The ADCP samples both the magnitude and phase of the returned echo, so the study could look at vertical migration rates from intensity data and measure vertical velocities from Doppler shift (Plueddemann & Pinkel, 1989).

While Pluedemann and Pinkel established that SSLs can be detected by ADCPs, Flagg and Smith (1989) published a pilot intercalibration study to show that ADCPs can measure zooplankton abundance. The study used a modified bottom-mounted narrowband 307kHz ADCP and a Multiple Open and Closing Net, with an Environmental Sensing System (MOCNESS) at the edge of the New England continental shelf. They showed a significant correlation between backscatter intensity from the ADCP and total zooplankton volume, and dry weight from the MOCNESS. The authors of this study showed that measurement of the abundance of zooplankton with an ADCP is possible, but argued that meticulous attention to the calibration of the ADCP as well as the quality of data from each profiler beam is necessary. Since the ADCP in this study was a narrowband instrument, the output was strongly temperature dependent and it was also necessary to know the temperature of the transducers for proper calibration (Flagg & Smith, 1989).

The ADCP in Flagg and Smith's study was adjusted to increase the maximum range and to process the incoming data slightly differently, leading to their argument that ADCPs must be altered to accurately measure zooplankton abundance. Heywood et al. (1991) used a standard narrowband 150 kHz ship-mounted ADCP to show that unmodified ADCPs are still useful in carrying out studies of zooplank-

ton abundance with intermittent net-tow calibrations. This is significant because of the large collection of unmodified ADCP data available from many oceanographic research cruises. The study compared biomass from net-tows in the top 200m with the summation of ADCP backscatter strength in the same water column in the Indian Ocean and found an encouraging correlation between the two (Heywood et al., 1991). A 1998 study that used 15 months of data from a bottom moored narrowband 300kHz ADCP described the SSL patterns of zooplankton at the edge of the eastern U.S. continental shelf. This study demonstrated the distinct advantage of ADCPs in continuous long-term measurements to reveal seasonal patterns (Ashjian et al., 1998).

Transition to Broadband ADCPs

While early studies utilized narrowband ADCPs, broadband ADCPs were shown to be more adaptable and have better data quality and began to replace narrowband ADCPs in the late 1990s (Wilson et al., 1997). The echo intensity outputs of the broadband ADCPs were not temperature dependent, as was the case for the transducers in narrowband ADCPs (Deines, 1999).

More recent studies using broadband ADCPs at various frequencies translate the echo intensity into volumetric backscatter using the sonar equation as first described by Deines (1999) and later corrected by Gostiaux and van Haren (2010) and Mullison (2017). There are several recent studies in various regions using this calculated volumetric backscatter to characterize SSLs and zooplankton abundance.

For example, the diel migration patterns of zooplankton in the South China Sea were observed by a 75kHz ADCP to understand seasonal variations as well as variations due to extreme events such as typhoons (Yang et al., 2019). A similar 2022 study in the Andaman Sea, which is the least-observed area in the Indian Ocean, used a bottom moored 75kHz ADCP to characterize migration behaviors and migration velocities of zooplankton and micronekton in relation to seasonal changes and monsoon effects (Liu et al., 2022). Other regional studies of seasonal migra-

tion variation have been carried out using moored ADCPs in many other locations including the Weddell Sea and the Lazarev Sea, Antarctica, the Arctic, and parts of the Mediterranean such as the Ligurian Sea (Berge et al., 2014; Bozzano et al., 2014; Cisewski & Strass, 2016; Cisewski et al., 2010).

1.5 Other Instruments

In addition to the ADCP data, this thesis benefits from several other instruments used during the CALYPSO 2022 field campaign. Temperature, salinity, dissolved oxygen, and chlorophyll measurements from the EcoCTD and MVP were compared to backscatter data in Chapter 3. In Chapter 2, the subsurface light was modeled using in situ measurements from a WireWalker and the pyranometer, which was on the *N/O Pourquoi Pas?*.

1.5.1 EcoCTD

The EcoCTD (Dever et al., 2020) was developed as part of CALYPSO specifically to study ocean dynamics and biophysical variability at submesoscales. It is a profiling instrument that can be deployed either in tow-yo mode, where it is dropped and then reeled back to the surface but not recovered for each profile, or in a single case mode where the instrument is recovered after each profile. It is capable of concurrently measuring hydrographic and bio-optical properties including oxygen, chlorophyll fluorescence, and optical backscatter. On the *N/O Pourquoi Pas*, the EcoCTD was deployed in tow-yo mode and required two personnel on deck during operation to manually reel out and retract the probe on an OceanScience UCTD winch that was mounted on the back of the ship. The EcoCTD probe is made of three instruments that sample at 8kHz: an RBR Concerto which measures conductivity, temperature, and pressure; a JFE-Advantech Rinko III that measures dissolved oxygen saturation; and a Sea-Bird Scientific WetLabs BB2F ECOPuck that measures backscatter at two wavelengths (470 and 700nm), and fluorescence

(see Figure 1-7) (Dever et al., 2020).

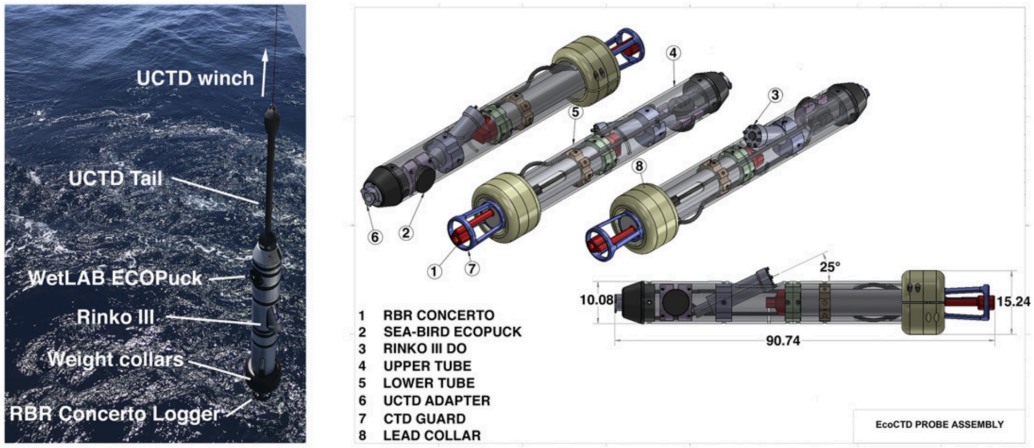

Figure 1-7: Left: EcoCTD probe being deployed from the NRV *Alliance* during a 2018 cruise in the Alborán Sea. Right: An engineering drawing of the EcoCTD design showing the key components and instruments of the probe. Reproduced from Dever et al., 2020.

During the CALYPSO 2022 campaign, we collected 2,795 EcoCTD profiles from the *N/O Pourquoi Pas?* to depths ranging from 160 – 250m. Following the cruise, the EcoCTD data was cross-calibrated with the shipboard CTD using data from four cross-calibration casts where the EcoCTD was mounted on the shipboard CTD (Middleton, 2023). Other quality control and filtering checks were run on the EcoCTD as described in the 2022 CALYPSO Data Report, the fully processed data was used in Chapter 3 of this thesis.

1.5.2 MVP

The MVP (moving vessel profiler) is a profiling instrument that is also deployed in a tow-yo mode, but this does not require personnel on deck, making it conducive for use during hazardous weather. The MVP had three sensors: one AML-X2 Change Conductivity-Temperature-Depth (CTD); one JFE-Advantech Rinko FT dissolved oxygen sensor; and one Turner Cyclops optical sensor (Middleton, 2023). The MVP was used for 362 profiles during the cruise to depths ranging from 150 – 212m when the EcoCTD could not be deployed due to technical issues or poor weather. The MVP was cross-calibrated with the EcoCTD and further processing

steps are included in the 2022 CALYPSO Data Report. In this thesis, the MVP data was used with the EcoCTD data for comparisons with backscatter in Chapter 3.

1.5.3 WireWalker

Two WireWalkers (Pinkel et al., 2011) were deployed during the 2022 CALYPSO Field Campaign. The WireWalker is a vertically profiling instrument package that is powered by ocean waves, it consists of a buoy at the surface with an instrument attached to a wire suspended from the sea surface. The instrument goes up and down along the wire and is powered by the motion of surface waves for descent and its own positive buoyancy for ascent (Pinkel et al., 2011). The WireWalkers for CALYPSO were used in a freely-drifting configuration to monitor the upper water column (down to 200m depth) with high-frequency sampling (Middleton, 2023). The WireWalkers were from the Center for Maritime Research and Experimentation (CMRE) and the University of Rhode Island (URI). Both were used on three separate deployments during the cruise.

The URI WireWalker was outfitted with two internally logging JFE Advantech DEFI2-L Photosynthetically Active Radiation (PAR) sensors, one on the surface buoy and one on the profiler. The data from the depth PAR was used in this thesis in Chapter 2 to calculate subsurface isolumes.

(a) (b)

Figure 1-8: The WireWalker being deployed from the *N/O Pourquoi Pas?* with the WireWalker on the left, and the buoy on the right. The WireWalker deployments were difficult evolutions requiring oversight and guidance from both technicians, Ben Hodges, and Drew Cole, as well as assistance from the ship's crew.

1.5.4 Pyranometer

The *N/O Pourquoi Pas?* has a suite of meteorological instruments mounted on the mast at about 10m above sea level. Included in this suite is a pyranometer, or sunshine sensor. The pyranometer measures solar irradiance, or incoming solar radiation. The measurements from the pyranometer were used to model subsurface light in Chapter 2 because the measurements are collocated with the ship .

Chapter 2

Sound Scattering Layers

2.1 Sound scattering layers (SSLs)

Sound scattering layers (SSLs) or deep scattering layers (DSLs) are vertically discrete water-column aggregations of organisms that can extend horizontally over thousands of kilometers (Proud et al., 2015). These concentrated layers of marine organisms extend 100m or less vertically and scatter acoustic energy (Plueddemann & Pinkel, 1989). They were first observed during World War II by naval sonars that detected DSLs and falsely identified them as sea bottom because they were so thick (Brierley, 2014). This early detection of SSLs demonstrates their continued operational importance to the submarine fleet of the United States Navy. An understanding of the SSLs in different areas of operation is essential for safety of navigation. In this thesis, SSLs that execute diel migrations are referred to as migrating scattering layers, while SSLs that remain at the same general depth are referred to as permanent scattering layers.

2.2 Diel Vertical Migration (DVM)

Diel vertical migration (DVM) is the synchronized up and down movement of zooplankton and fish in the water column over a daily cycle (Brierley, 2014). DVM

was documented very early on, beginning with an observation from a cruise that took place from 1819 – 1821 in the Southern Ocean, where the explorer Bellingshausen noted that salp and other luminescent plankton “were caught only when it was dark.” Later, evidence from the Challenger expedition (1872 – 1876) indicated that vertical migration was a common pattern of behavior in planktonic organisms, with specific observations of copepods (Bayly, 1986).

DVM is seen in marine and freshwater pelagic communities and involves a diverse array of marine species. The acoustic properties of the water column are dramatically altered by DVM, making it essential to characterize these patterns for both physical oceanographers to allow for this variance, and for biological oceanographers who seek to explain this behavior.

2.2.1 Types of DVM

Three major patterns of DVM have been identified: nocturnal migration, twilight migration, and reverse migration (Tarling et al., 2001). Nocturnal migration is the most commonly identified type and is the pattern seen in the following analysis in section 2.4. In nocturnal migration, the organisms ascend at sunset and descend at sunrise, spending the night at a shallower depth, and migrating to deeper depths where they stay during daylight hours. Twilight migration involves two separate migrations during a 24-hour period: first, an ascent to the surface at sunset, then a descent to deeper water around midnight, called the “midnight sink”, followed by a second ascent to the surface and then a descent to deeper water at sunrise (Cisewski et al., 2010). The third pattern, reverse migration, occurs when organisms ascend to shallow water at sunrise and spend the day in shallower water, then descend at sunset to spend the night in deeper water (Bayly, 1986).

2.2.2 Drivers of DVM

The leading and most widely supported hypothesis in the literature for the evolutionary advantage of DVM is reduced mortality risk by predator avoidance (Cohen

& Forward Jr, 2002). For the nocturnal and twilight DVM patterns, the organisms take daytime refuge from visual predation by spending the daylight hours at depth, where there is less sunlight available, and migrate upward at night to feed on photosynthesizing organisms that are abundant at the surface. The reverse DVM pattern would provide protection from nocturnally migrating predators which is useful to some species. The current literature points to change in light intensity as the proximate cue, or trigger, for DVM (Brierley, 2014). The evidence for this includes that migration usually occurs at twilight which is the time of day with the greatest change in irradiance, and that some zooplankton species maintain depth at distinct levels of irradiance, or specific isolumes (lines of constant light) throughout the diel cycle (Cohen & Forward Jr, 2002). Changes in local light intensity such as from storms, eclipses, and full moons have also been shown to elicit a response in the DVM pattern. It has even been shown that nocturnally migrating organisms at their daytime depths are constantly swimming in response to cloud-driven light variations at the sea surface (Omand et al., 2021).

2.2.3 Importance of DVM

DVM is thought to be the largest natural daily movement of biomass on the planet. Individual migrators can swim tens to hundreds of meters in just a few hours, a remarkable distance for small animals that are on the mm to cm scale. These tiny organisms make this movement every single day in nearly every body of water on Earth. Just the sheer magnitude of DVM is dizzying, but the importance goes far beyond the impressiveness of tiny organisms making such a monumental trek.

Zooplankton make up a large part of the organisms that vertically migrate and are also an extremely important base to marine ecosystems. Understanding the variability of zooplankton biomass is essential for our basic understanding of marine ecosystems, and to our understanding of the effects of climate change on ecosystems. This has important implications for worldwide fisheries and consequently has major implications for human health and economies in many parts of the world.

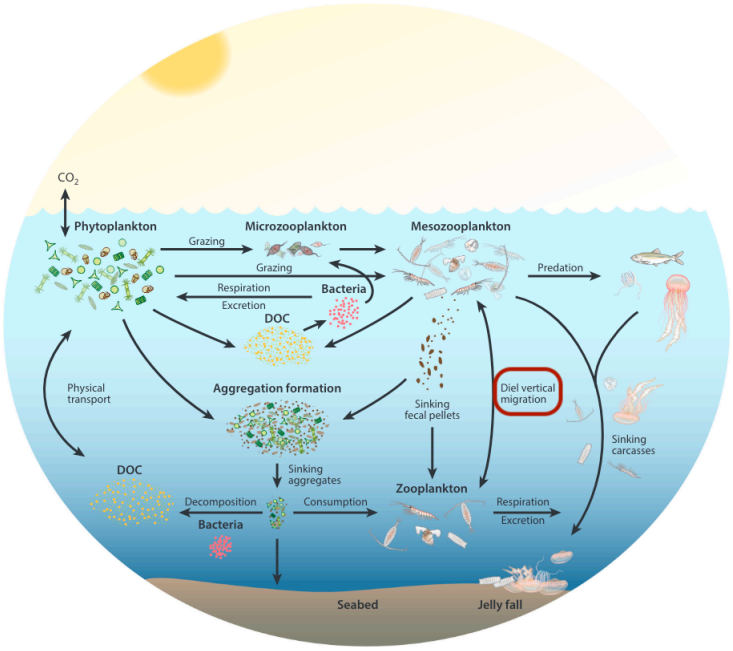

Figure 2-1: The pathways of cycling and export of carbon by zooplankton in the ocean. Diel vertical migration (outlined in red) is a major component in which migrators feed in surface waters at night and metabolize the food they ingested in the mesopelagic zone during the day, then swim to deeper depths where they respire and excrete. Reproduced from Steinberg and Landry, 2017.

Biological Pump

Zooplankton have a significant effect on the biological pump, the suite of biological processes that mediate the transport of carbon from the upper ocean to depth. These processes are illustrated in Figure 2-1. Zooplankton play many roles in the cycling and export of carbon in the ocean, and DVM is one of those important roles. As a component of the biological pump, DVM is referred to as active transport to distinguish it from the passive sinking particles. Particulate organic carbon (POC) is respired by zooplankton as CO_2 and excreted as dissolved organic carbon (DOC). The migrators transfer some of the POC that was ingested in surface waters during the night through respiration or excretion at daytime residence depths below the euphotic zone. This flux can be significant compared with sinking POC flux. The death of diel migrators at depth is an additional flux to the deep ocean.

The magnitude of active transport through DVM varies regionally and seasonally

depending on the migrator biomass, taxonomic composition, and variations in DVM patterns and is not well quantified (Steinberg & Landry, 2017). One modeling study used satellite data to try to quantify the impact of zooplankton DVM on the carbon export flux of the biological pump. They found that with DVM the carbon export flux from the base of the euphotic zone was 6.5 PgC/year which is 14% higher than when the model is run without DVM, demonstrating the strong effect that DVM has on the carbon cycle (Archibald et al., 2019). Understanding the variations in carbon flux and quantifying the effects of DVM can help to parameterize biogeochemical models of the biological pump as well as help us understand the potential effects of climate change on the ocean carbon cycle.

2.3 Methods

2.3.1 ADCP Echo Intensity Data

The echo intensity data from the three ship-mounted ADCPs onboard the *N/O Pourquoi Pas?* were used in this data analysis. In order to calculate current velocities from Doppler shift, the ADCPs collect echo intensity which is the strength of the reflection of scatterers in the water column. The sonar equation was applied to the raw echo intensity data to calculate the Mean Volume Backscattering Strength (MVBS or S_v).

2.3.2 Mean Volume Backscattering Strength (MVBS or S_v)

The Mean Volume Backscattering Strength (MVBS or S_v) was calculated for the data from the 38kHz, 150kHz, and 300kHz ADCPs. The MVBS provides a relative measurement of scattering strength to better quantify the abundance and distributional patterns of suspended matter that are the sound scatterers for broadband ADCP measurements (Deines, 1999). The original MVBS calculation and information on calibrating ADCPs to achieve backscatter measurements were published in 1999 by RD instruments (Deines, 1999). An error in the signal-to-noise term

in the original equation, which results in erroneous backscatter estimates for data sets with known low backscatter concentrations, was corrected in 2010 (Gostiaux & van Haren, 2010). This error was addressed with a correction by Teledyne RD Instruments in an Application Note in July 2017 (Mullison, 2017). The MVBS calculations in this study are made using the corrected signal-to-noise term. The updated volumetric backscatter equation from Mullison is:

$$S_v = C \ + \ 10 \ \log_{10}((T_x + 273.16)R^2) \ - \ L_{DBM} - P_{DBW} + 2\alpha R \ + \ 10 \ \log_{10}(10^{k_c(E-E_r)/10)} \ - \ 1). \quad (2.1)$$

Here, C is a constant made up of several parameters specific to each ADCP; it is included because MVBS is a relative measurement. T_x is the temperature measured at the transducer. R is the along-beam range to the instrument. L_{DBM} is $10\log_{10}$ of the transmit pulse length in meters, which depends on the setup of the instrument. P_{DBW} is $10\log_{10}$ of the transmit power in Watts, which is calculated from the recorded transmit current and voltage. The acoustic absorption, α, is the only variable that cannot be directly measured by the ADCP. It is based on the characteristics of the seawater and differs based on water basin temperature and salinity and the frequency of the instrument. E is the measured Returned Signal Strength Indicator (RSSI) amplitude from the ADCPs in counts. E_r is the noise in counts and is constant for any given ADCP.

For this work, a simplified version of equation 2.1 was applied to the ADCP echo intensity data. Specifically, C, L_{DBM}, and P_{DBW}, which are specific to the ADCP instrument, were omitted as they do not significantly affect the relative calculations and are constant values. The ADCPs were not calibrated for amplitude, so the echo intensity data is relative to begin with. The modified sonar equation used to translate the echo intensity into MVBS is given by:

$$S_v = 10\log_{10}(R^2) + 2\alpha R + 10\log_{10}(10^{E-E_r/10}). \quad (2.2)$$

The first term in equation 2.2 and second term in equation 2.1 represent spherical spreading. In equation 2.2 we neglect temperature because it has a negligible effect on the backscatter intensity for broadband ADCPs. R is the along beam range to the instrument and can be calculated with the beam angle, θ, and the size of the depth cell, D. Both θ and D were found in the leader data for the raw ADCP data. The range is calculated using the equation:

$$R = \frac{R_1 + D/4 + (n-1)D}{\theta}. \tag{2.3}$$

Absorption of seawater, or the conversion of acoustic energy into heat due to shear and bulk viscosity, heat conduction, and a relaxation mechanism, is quantified by the absorption coefficient, α (dBm^{-1}). More specifically, the absorption coefficient of seawater is affected by boric acid ionization, magnesium sulfate ionic relaxation of molecules, and pure-water absorption due to shear and volume viscosity. These mechanisms describe the effects of salinity on absorption and differ based on the frequency of the instrument. Each mechanism is also affected by temperature and pressure. The factors affecting the absorption coefficient and the associated frequencies are described in more detail in table 2.1.

Mechanism	**Type**	**Frequency**
Boric Acid Relaxation	low frequency relaxation	$\leq$ 10kHz
Magnesium Sulfate ionic relaxation	high frequency relaxation	$\leq$ 1000kHz
Pure-water absorption	shear and volume viscosity	$\leq$ 100kHz

Table 2.1: The absorption mechanisms that affect absorption in seawater and contribute to the calculation of the absorption coefficient α, the frequencies that they affect, and the physical parameter that they are a function of as described by Francois and Garrison, 1982a, 1982b.

Absorption contributes to the transmission loss of sound from the transmitter to the receiver, so the spherical spreading and cylindrical spreading terms in the sonar equation include α, but α is a smaller contribution than the spreading of the acoustic wave. For the sonar equation calculation in this work, the α is included

in the spreading term. Here we are concerned only with the effects of boric acid relaxation and pure-water absorption because magnesium sulfate ionic relaxation only affects absorption at much higher frequencies. The absorption coefficient for the ADCPs was calculated using a MATLAB routine based on the equations from Francois and Garrison, 1982a and Francois and Garrison, 1982b which take into account ambient temperature and salinity, pressure, and ADCP frequency.

The EcoCTD measurements of temperature range from 13.5 – 14.5 $^{\circ}$C and the salinity ranges from 38.4 – 38.8 psu. For the 38kHz ADCP, the first 600m of data is used for analysis, the first 400m is used for the 150kHz ADCP, and the whole range of 140m is used for the 300 kHz ADCP. The α is calculated for each depth, temperature, and salinity with a range of 0.0518 – 0.0572 for the 150kHz data, a range of 0.0095 – 0.0104 for the 150kHz data, and a range of 0.0853 – 0.0867 for the 300kHz data. The attenuation coefficients are all small with a small range of variation, so nominal values using the average temperature, salinity, and pressure values for the data range are used to calculate α = 0.0554 for the 150kHz ADCP, α = 0.0101 for the 38kHz ADCP, and α = 0.086 for the 300kHz ADCP. The third term in equation 2.2 and the final term in equation 2.1 is the signal-to-noise ratio. The k_c term in equation 2.1 is the scaling coefficient to convert echo intensity from counts into decibels. During data processing, the CALYPSO ADCP data was converted from counts to decibels; therefore, the k_c and -1 are unnecessary when applying the sonar equation.

In equation 2.2, E is the raw echo intensity in decibels and E_r is the noise level in decibels. The noise level is estimated for each ADCP by visually plotting the amplitude versus range, and estimating the drop off in amplitude for a representative sample of pings. We estimate the E_r to be 15dB for the 150kHz ADCP and 10dB for the 38kHz and 300kHz ADCPs. Figure 2-2 shows an example of the echo intensity with the estimated noise removed for the 150kHz ADCP.

The MVBS is calculated for all three ADCPs for every single ping to better understand the visual patterns of scatterers in the Balearic Sea during the study period. The sonar equation is applied to the average of the echo intensities from all four

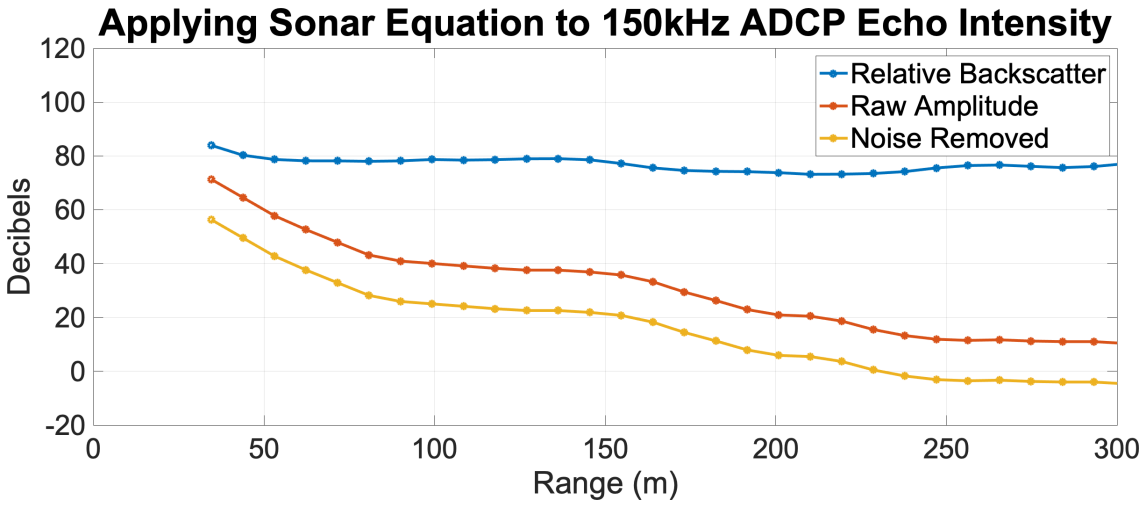

Figure 2-2: The original raw amplitude or echo intensity for one ping in the 150kHz ADCP data is in orange, the yellow line is with the noise removed, and the blue line is the calculated MVBS or relative backscatter which is the result of applying the sonar equation (equation 2.2) to the ADCP data. This illustrates the effect of the sonar equation for a single ping.

beams for each ADCP. The four beams are compared for any outliers, but no additional corrections are applied to the echo intensity measurements. Figures 2-3a, 2-3b, and 2-3c show a representative six-day sample of the MVBS for all three ADCPs from March 1 to March 6. A sinusoidal pattern is indicative of DVM as the distribution of biomass with depth through time has been shown to follow a sine curve (Ashjian et al., 1998). This sinusoidal pattern is visible in the 38kHz MVBS, but further data analysis was carried out to better understand if this was indicative of DVM. There are some less visible daily patterns in the 300kHz and 150kHz MVBS. Of note, the 300 kHz ADCP only had a depth of 140 meters while the 150kHz went down to 440 meters and the 38kHz ADCP had a range of 800 meters. These depth ranges differ due to the different frequencies of the instruments.

Together, these three frequencies cover the water column from 10m – 800m. Although they detect different sizes of organisms, together they can provide a collective characterization of the SSLs in this region and season. We tried plotting all three in one figure by taking the antilog, adding them together at each depth, and then multiplying by $10 \log_{10}$. However, as mentioned earlier the ADCPs have not been calibrated to properly compare between frequencies, and the resulting

figures do not provide any new insight into the SSLs. Therefore, the SSLs are characterized by considering each frequency individually.

2.3.3 Sunrise and Sunset Times

The sunrise, sunset, and high noon times were calculated with the ship's location using a MATLAB routine to understand if the time of sunrise and sunset affected the DVM patterns (Beauducel, 2023). The sunrise time was 32 minutes earlier on the last day of the cruise than the first day and the sunset was 24 minutes later on the last day as opposed to the first. On a daily time scale, the time of sunrise and sunset would slightly offset the isolumes which would likely affect the migration time (discussed more in section 2.3.6). However, we determined that this time shift did not have a statistically significant effect on the overall DVM pattern when considering the 12-day time frame discussed here. Therefore, we binned the average MVBS along time of day using the two-minute interval consistent with the two-minute ADCP sampling rate.

2.3.4 Daily Composite (S_D)

We narrowed the time window to twelve days of data from February 27 to March 10 before calculating the daily composite. The 300 kHz ADCP had been added to the *N/O Pourquoi Pas?* specifically for the CALYPSO cruise in order to target the current velocities in the upper 25 meters which are difficult to measure due to the ship's wake. Unfortunately, the 300kHz ADCP did not start working properly until several days into the cruise. The echo intensity data for the 150kHz and 38kHz ADCPs are very noisy during the first few days as well, likely due to acoustic interference during instrument testing. This 12-day time frame selection is a representative example of the cruise.

S_D is the daily composite. It was calculated by averaging the MVBS across

every day during the 12-day time frame in two-minute bins using the relationship,

$$S_D(tod, z) = \overline{S_v}^{tod}(t, z), \tag{2.4}$$

where 'tod' stands for time of day. The result is an average of the daily patterns of the SSLs over a 24-hour day, including the deep scattering layers and migrating layers.

2.3.5 MVBS Anomaly (S_0)

The original MVBS calculation and the daily composite, S_D, resulted in a consistent sinusoidal pattern indicating the occurrence of DVM across the study region (Ashjian et al., 1998). To separate the permanent scattering layers from the migrating layers, we took a mean profile of the daily composite and subtracted it from the original daily composite S_D to find the MVBS anomaly using the equation:

$$S_0(tod, z) = \overline{S_m}(z) - S_D(tod, z). \tag{2.5}$$

S_m is the mean MVBS profile of the daily composite, S_D. S_0 is the resulting MVBS anomaly as a function of time of day and depth.

These three variables are plotted in Figures 2-4 and 2-5 for the 38kHz and 150kHz ADCPs respectively. S_D reveals a distinct DVM pattern in the 150kHz and 38kHz MVBS. The blue bowl-like shape indicates an absence of scatterers during the daylight hours and the yellow color indicates high volumetric scattering or the presence of many scatterers. This indicates that DVM is occurring in the Balearic Sea during the study period. However, it is not possible to see where the scatterers may have migrated to. The S_0 for both frequencies reveals a clear pattern of more scatterers at the surface during the night and more scatterers at depth during the day.

2.3.6 Light Intensity

Through the MVBS and daily composite calculations we have shown that a daily pattern exists that is roughly consistent with the nocturnal DVM pattern where organisms migrate to depth during the daytime and back to the surface at night. Since the driver of DVM is light (discussed in section 2.2.2), we want to take a closer look at the migrating patterns and see if they are responding to the sunlight for each specific day. The measures of sunlight during the 2022 CALYPSO cruise included the PAR sensor on the URI WireWalker (section 1.5.3), and the pyranometer that is located in the meteorological instrument suite on the *N/O Pourquoi Pas?* (section 1.5.4). The solar angle was also calculated during the cruise period using the location of the ship in a solar calculations MATLAB routine (Dozier, 2023).

The calculated solar angle, the pyranometer data, and the raw WireWalker PAR data all lined up well with the blue-bowl like features in the 38kHz and 150kHz MVBS which were during daylight hours and are indicative of fewer scatterers (the space the organisms left empty when they migrate to depth). This result confirmed that the migrators are spending the day at depth. However, we wanted to see how the migrators react to specific isolumes. To model the subsurface light, we use the WireWalker PAR data and the shipboard pyranometer data using a method similar to that described in Omand et al., 2021 and Zheng et al., 2023.

The PAR below the surface was modeled as decaying exponentially in depth using the equation:

$$I(z) = I_0 e^{-kz}. \tag{2.6}$$

I_0 is the incoming solar radiation measured from the pyranometer, k is the diffuse attenuation coefficient of irradiance, and z is depth. Two attenuation coefficients were calculated from the WireWalker profiles from linear fits of $\ln[I(z)]$ in relation to depth. There are two distinct profiles, each with an attenuation coefficient, one in the first 50 meters, and the second from 50 – 75 meters. We calculate the linear fit for every WireWalker profile for each attenuation coefficient and we select the median value for the model. For the top 50m, k_1 is 0.0442, and from 50 – 75m, k_2

is 0.02275.

The euphotic depth (Z_{eu}) is the depth where PAR is 1% of the surface value. Using the k_1 value, it is estimated to be 104m using equation:

$$Z_{eu} = \frac{-\ln 0.01}{k}. \tag{2.7}$$

A larger absolute Z_{eu} means that the water is clearer because the light is able to penetrate more deeply (Zheng et al., 2023). The euphotic layer of 104m is fairly deep when compared to other oceans, but the Mediterranean Sea is oligotrophic and a deeper euphotic layer makes sense as there are lower nutrients at the surface.

To model the PAR below 50m, we calculate I_0 at 50m using equation 2.6 and modifying it to:

$$I(z) = I_{50}e^{-k_2(z-50)}. \tag{2.8}$$

This model results in the isolumes visible in panel c in Figure 2-6. Panel d in the same figure is the 38kHz MVBS S_0 with the isolumes overlaid, here it is clear that the scatterers perform downward and upward migration along the isolumes. In some cases, such as on March 5 (see Figure 2-7), the scatterers appear to follow the isolumes very closely, even swimming back up when there is lower light. The variability from day to day also matches up well with the variability of the modeled isolumes. However, the small changes on a minute-to-minute time scale do not always match up exactly with the differences in backscatter. We modeled this analysis after a 2021 study that showed migrating organisms respond to cloud-driven variations at the deep scattering layer (Omand et al., 2021). While some evidence of this is visible here, such as in Figure 2-7, our ADCP data was not binned to as fine of a time scale and has a lower resolution. It is clear from the isolumes in panel d of Figure 2-6 that the migrating layers are following the isolumes at sunrise and sunset when they conduct their daily downward and upward migrations, supporting the hypothesis that light is a cue for migration.

2.3.7 Speed of Vertical Migration

The average swimming speed of ascent and descent of the scatterers is estimated as a function of depth for the 150kHz and 38kHz MVBS using the S_0 (panel c) from Figures 2-5 and 2-4. Since S_0 is the anomaly from the time mean at every depth it represents the migrating layers. The swimming velocities are calculated using a best-fit line to calculate the slope of the transition from red to blue. The transition between the positive anomaly and negative anomaly of backscatter represents where the majority of scatterers are vertically migrating. There are clear gradients in both the 38kHz and 150kHz ADCP, however, they differ between frequencies and between upward and downward migrations. The 150kHz ADCP has two distinct layers of migrating organisms that the speed of vertical migration was calculated for: one where migrators swim downward from 50m to about 75m and a second layer where migrators swim downward from about 100m to 250m. While the upper layer is barely visible in the 38kHz MVBS, the deeper layer is easy to distinguish and the vertical migration speed was only calculated for the deeper layer.

2.4 Results

2.4.1 Scattering Layers

Permanent Scattering Layer

The calculation outlined in section 2.3.5 reveals a deep scattering layer in both the 38kHz MVBS and 150kHz MVBS from about 350 meters to 450 meters. This is clear when the mean profile, S_m, is removed from the original daily composite to get S_0. The bright yellow and green bands visible in panel a in Figure 2-4 from 300m – 440m, and in Figure 2-5 from 300m – 500m is the permanent deep scattering layer. Interestingly, the permanent scattering layer in the 38kHz ADCP displayed more day-to-day variability than in the 150kHz ADCP. This is visible in Figure 2-3 in panels b and c. It is not possible to tell if this day to day variability is due to changing

isolumes, isopycnals, or another parameter because the CALYPSO 2022 data set does not include measurements of salinity, temperature, chlorophyll, or DO to this depth. In the 150kHz MVBS, the permanent scattering layer is constant at 350m – 440m from day to day, it is possible that this is due to the limits of the 150kHz ADCP since 440m is the extent of its range. The backscatter at the end of the range may not be as precise as the sound is more affected by attenuation and spreading the further it is from the transducer.

Even though the permanent scattering layers are removed to understand the DVM patterns for this work, it is an important feature to identify both for scientific understanding and for operational characterization of the environment, particularly in the use of Navy sonar systems. This analysis shows that the deep scattering layer can be detected by commonly used ADCPs at multiple frequency bands. Although this analysis cannot discern specifically which scatterers make up the deep scattering layer, understanding that it is a regional characteristic can be essential for sonar operations.

Migrating Layers

The migrating layers in the 38kHz and 150kHz ADCP are visible in panel c in Figure 2-4 and Figure 2-5. Once the permanent scattering layers are removed from S_v as the mean profile, S_m, the anomalies reveal daily patterns which are consistent with nocturnal DVM where zooplankton and micronekton swim to depth during daylight hours and swim to the surface at sunset to feed during the night. For the 38kHz there is a distinct blue bowl-like feature during daylight hours. The blue indicates the absence of scatterers, there are two separate layers, one at the surface to about 50m and one from 150-250 meters. The dark red color at the surface and from 150-250 meters during the nighttime indicate higher levels of scatters at the surface. With the permanent scattering layer removed it is clear that scatterers migrate to depths below 250m. The higher scatterers at depth during the day are more spread out; this is likely due to the scatterers being further apart as they are not actively grazing. An acoustic phenomena called acoustic extinction may also

be at play, this occurs when energy is taken out of the forward-propagating incident wave and is a known affect in bioacoustics, especially when detecting organisms in schools or swarms versus when they are dispersed.

The 150kHz S_0 also reveals two migrating layers. The surface migrating layer is more visible in the 150kHz MVBS than in the 38kHz MVBS, likely due to the higher resolution near the surface expected from the 150kHz ADCP. The high scattering strength in red begins in the top 50m during the night and migrates about 50m down to the 100m – 150m range, leaving a small blue bowl-like feature at the surface during the day. The second migrating range is also visible, with a secondary blue bowl-like feature from 150m – 250m during the day. These layers are consistent between the 38kHz and 150kHz MVBS, however, the different frequencies detect different scatterers, which accounts for the differences in the MVBS anomaly plots. The higher-frequency 150kHz ADCP has been shown to detect zooplankton such as copepods and krill (Pinot & Jansá, 2001). We expect the 38kHz ADCP to mostly detect pelagic fish and some larger zooplankton.

2.4.2 Speed of Vertical Migration

Several previous studies have calculated the speed of vertical migration of specific species using a combination of ADCP data and net tows. One 2001 study in the Western Mediterranean Sea used a ship-mounted 153kHz ADCP and a $1m^2$ MOCNESS to capture and quantify zooplankton biomass while the ADCP was running (Tarling et al., 2001). The net samples which were taken at discrete depths, showed that the zooplankton community was dominated by two species, Northern krill (*Meganyctiphanes norvegica*) and pteropods (*Cavolinia inflexa*). The biomass of these two species was calculated at distinct depths at varying times during the eight-day study. The depth-discrete biomass was then correlated with the migrating layers found in the ADCP data and the authors were able to estimate swimming velocities for Northern krill and pteropods. The pteropods had an upward speed of 2 – 7cms^{-1} and a downward speed of 4 – 7cms^{-1}. The Northern krill was found to

have an estimated upward migration speed between 7 – 8cms^{-1} and a downward migration speed of over 11cms^{-1} (Tarling et al., 2001).

We found migration speeds of 2 – 11cms^{-1} in the 38kHz MVBS migrating layer, but lower swimming speeds of 1 – 2cms^{-1} in the 150kHz MVBS. This disparity is unexpected because previous studies have calculated swimming speeds using 150kHz ADCPs (Tarling et al., 2001). The difference might be due to differences in the measurements from the two ADCPs; the 38kHz ADCP generally had stronger backscatter measurements making it easier to identify DVM and to extract the migrating layers from the background. Additionally, because of the depth range of the 38kHz ADCP, the full vertical migration slope was measured whereas the signal for the 150kHz backscatter drops off more quickly.

The 38kHz vertical migration speeds are plotted as a function of depth in Figure 2-8. The bold orange line shows the average downward (dawn) migration and the dotted orange lines are the daily migrations of a selection of four days to indicate the day-to-day variability. The blue solid line is the upward (dusk) migration speeds with day-to-day variability in the dotted blue lines in the background. Our calculations yielded a slightly asymmetrical pattern of migration speed where the upward migration is slower than the downward migration. This could either be due to sinking helping organisms migrate downward faster, or due to the difference in swimming orientation of organisms. As discussed in 1.4.2, the swimming orientation of organisms affects the target strength and can consequently affect the backscatter data.

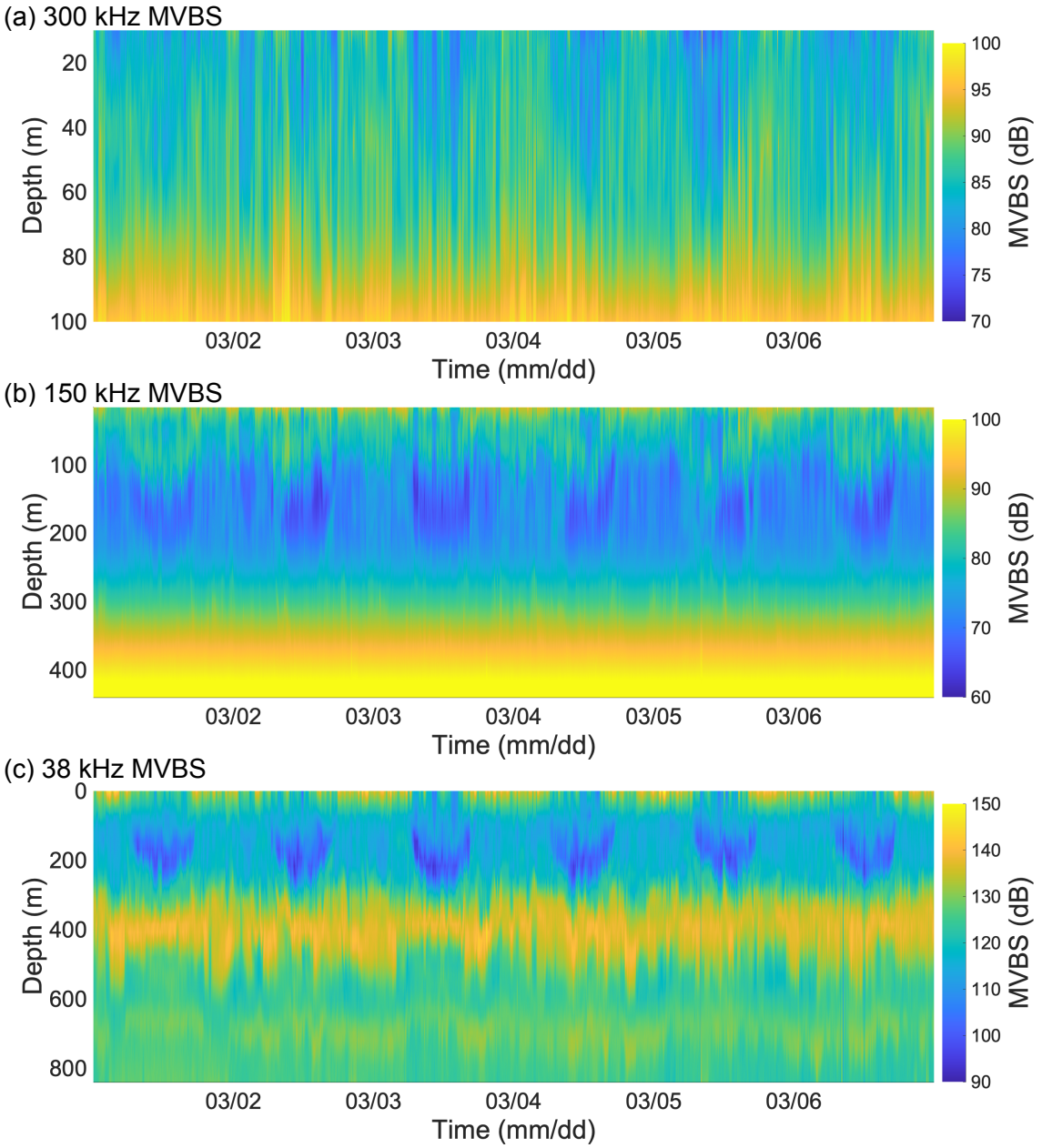

Figure 2-3: Calculated MVBS for the 300kHz (panel a), 150kHz (panel b), and 38kHz (panel c) ADCPs which were mounted on the *N/O Pourquoi Pas?*. A six-day period from March 1 to March 6 is shown as a representative sample of the daily pattern seen throughout the 12-day study period. Note that the y-axes representing depth are different at each frequency due to the difference in the instrument ranges. The 300kHz ADCP measured to 140m, the 150kHz to 440m, and the 38kHz to 800m. The colorbars also differ because the target strength measured by each instrument differs, but in all three the yellow indicates a relatively higher volume of backscatterers while blue indicates a lower volume of backscatterers. All three frequencies reveal a daily pattern, visible in the blue, or lower scattering areas seen relatively near the surface during the daytime for each. This pattern is strongest in panel c.

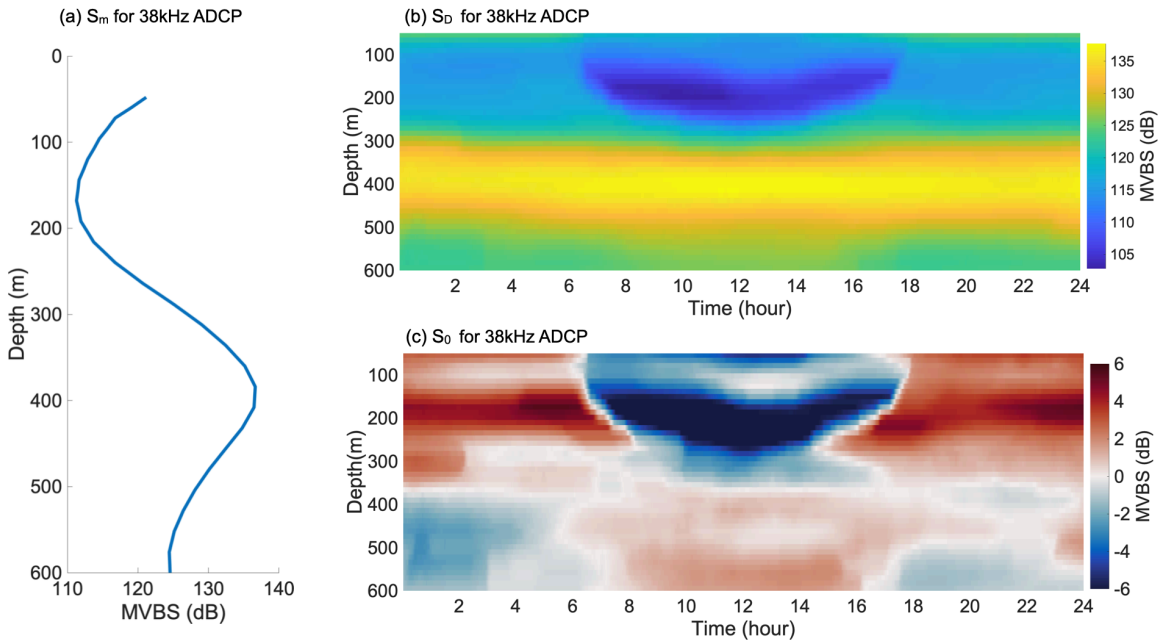

Figure 2-4: The S_m, S_D, and S_0 for the 38kHz ADCP. The S_D in panel b is the daily composite for the 38kHz MVBS, it is the average of the MVBS every 2 minutes for all 12 days of the study period plotted over 24 hours. The blue bowl-like shape indicates the absence of scatterers during the day time. The bright yellow stripe is an area of high backscattering strength that does not vary considerably over the day and is considered a permanent scattering layer. The S_m in panel a is the mean MVBS profile for the daily composite, when subtracted from panel b the result is panel c where the migrating layers are visible. The red represents levels of high backscattering strength while the blue represents areas of low backscattering strength. The blue bowl-like shape is still visible in the S_0 and an area of high backscatter is visible at depths during the daylight, indicating a DVM pattern.

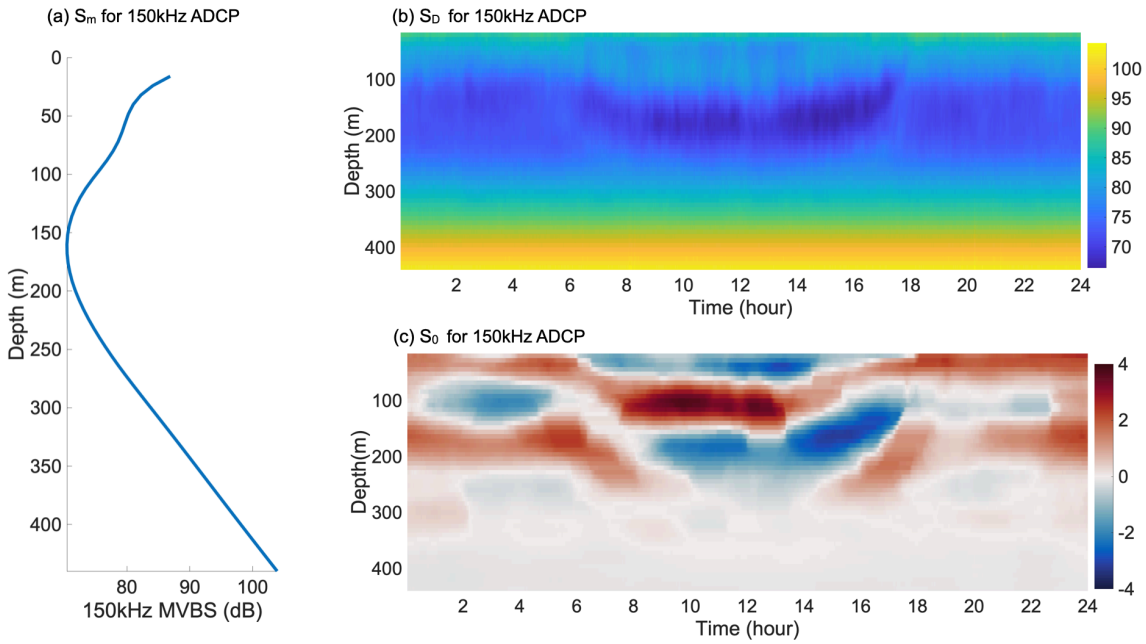

Figure 2-5: The S_m, S_D, and S_0 for the 150kHz ADCP. The S_D in panel b is the daily composite for the 150kHz MVBS, it is the average of the MVBS every 2 minutes for all 12 days of the study period over 24 hours. The blue bowl-like shape indicates the absence of scatterers during the day time. The bright yellow stripe starting at around 380m is an area of high backscattering strength that does not vary significantly, so it is considered a permanent scattering layer. The S_m is the mean MVBS profile in depth for the daily composite. When S_m is subtracted from panel b, the result is panel c where the migrating layers are revealed. The red represents levels of high backscattering strength while the blue represents areas of low backscattering strength. The blue bowl-like shape is still visible in the S_0 and an area of high backscatter is visible at depths during the daylight, indicating a DVM pattern.

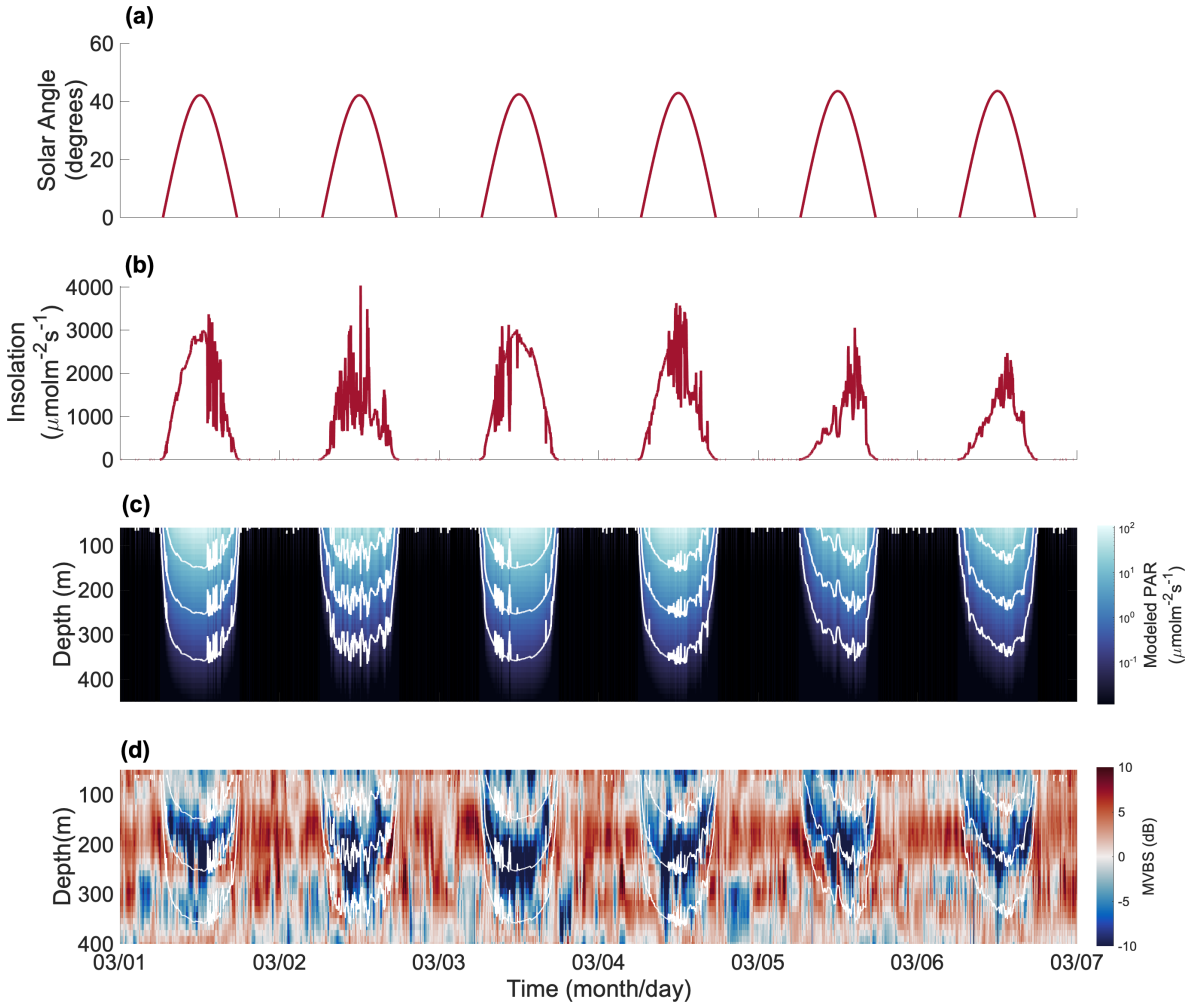

Figure 2-6: The various measurements of sunlight used in this study over a six-day period from March 1 to March 6. Panel a is the calculated solar angle in degrees. Panel b is the raw incoming solar radiation converted from Wm^{-2} to μmolm^{-2}s^{-1} measured by the pyranometer that is part of the meteorological instrument suite onboard the *N/O Pourquoi Pas?*. Panel c is the modeled subsurface PAR and isolumes calculated using equation 2.8. The isolumes are 0.1, 0.01, and 0.001 from the surface down. Panel d is the modeled isolumes overlaid on the 38kHz backscatter anomaly S_0. Panels a, b, and c all line up in time with the sinusoidal pattern of scatterers in the 38kHz backscatter anomaly. Panel d shows that the backscatterers travel along the isolumes (the transition from blue to red) during the downward migration at sunrise and back up the isolumes at sunset.

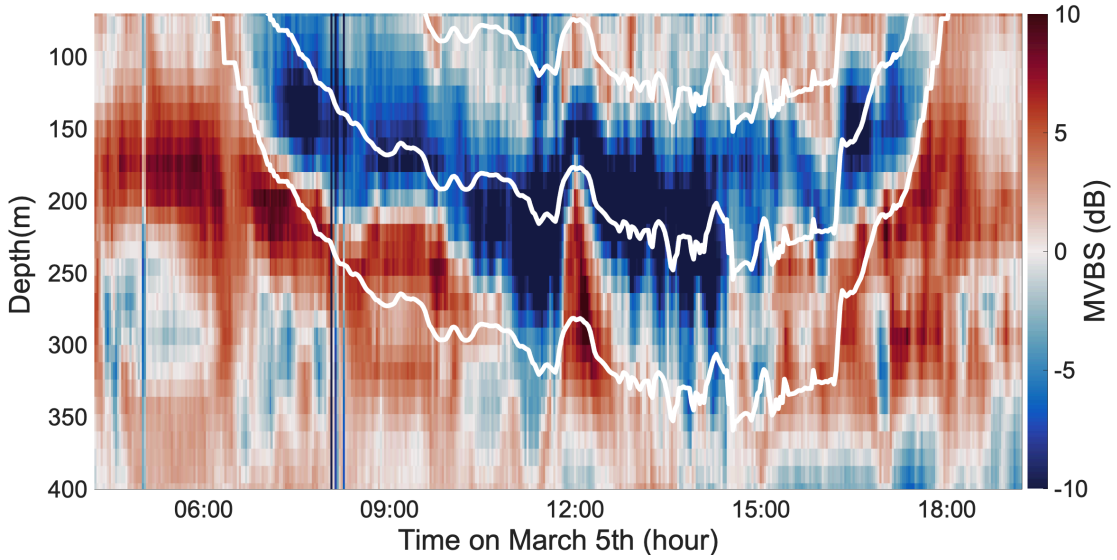

Figure 2-7: A closer look at the 38kHz backscatter anomaly with modeled isolumes overlaid on March 5 from panel d in Figure 2-6. The isolumes are 0.1, 0.01, and 0.001 from the surface down. There is a close correlation of the scatterers along the 0.001 isolume during the sunrise hours when they descend and ascend at sunset. There is an interesting variation at 12:00 where the 0.01 isolume decreases and there is a corresponding spike in the migrators swimming upwards.

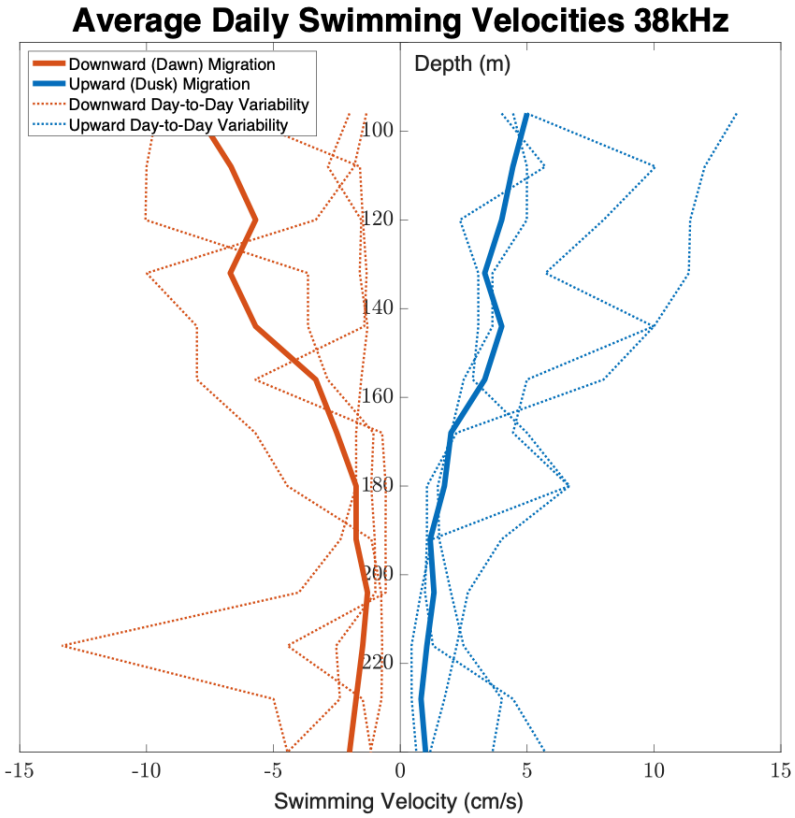

Figure 2-8: Speed of vertical migration of scatterers measured by the 38kHz MVBS. The orange lines are the downward (dawn) migration and the blue lines are the upward (dusk) migration. The bold lines represent the average speed over all days, calculated from S_0, and the dotted lines represent calculations from four individual days to show day-to-day variability of migration speeds.

Chapter 3

Frontal Variability

3.1 Methods

The CALYPSO 2022 field campaign was designed to sample submesoscale features including eddies, fronts, and filaments, using an adaptive sampling approach. As previously described in section 1.2.1, the three phases of the cruise included sampling of an area of deep convection (Phase 1), a high chlorophyll cyclonic eddy that elongated into a ridge and collapsed into two smaller eddies (Phase 2), and another cyclonic eddy that had entrained a filament of colder water (Phase 3). To achieve this sampling plan, the *N/O Pourquoi Pas?* traversed back and forth across lateral density gradients to sample physical and biological parameters several times.

This resulted in a unique data set of 255 individual transects. The transects are differentiated by the direction of the ship so that for each new transect the ship was on a new heading. The transects covered every part of the *N/O Pourquoi Pas?'s* track, but there is not EcoCTD or MVP data for every transect. The EcoCTD was deployed to measure salinity, temperature, oxygen, chlorophyll, and optical backscatter in the vertical and horizontal when the ship was steaming between 4 and 6 knots and when weather permitted. The transects where CTD deployments took place are not included in this analysis as the ship had to be dead in the water to

deploy the rosette. There are also some gaps in the EcoCTD data due to equipment issues or dangerous weather conditions.

The following analysis only focuses on transects where there is EcoCTD data during the time period from February 27 to March 10 which has the best representation of ADCP data. The latitude and longitude of each transect was translated into distance along track in kilometers for better visualization using a MATLAB routine (Greene, 2023). All times are in UTC. In this chapter, we compare the EcoCTD parameters with the MVBS to understand frontal or horizontal variability of the scatterers.

3.1.1 MVBS or S_v

In Chapter 2 we calculated the MVBS anomaly for the daily composite, or S_0. This was useful for identifying the DVM patterns overall, however, for this chapter, we seek to compare the MVBS to EcoCTD parameters on a finer, day-to-day scale. Rather than using the daily composite S_D, we use the S_v for every day and find that there are three possible ways in which we coan look at how backscatter varies. First, there is how the DVM varies from day to day which is the S_v minus the mean MVBS resulting in the S_0 for the entire data set. Next, how the permanent scattering layers vary would be determined by subtracting just the DVM variations from the S_v for the whole data set. Finally, to determine how backscatter varies on a fine scale at a specific transect, we use the equation:

$$S_n(x,z) = S_{v_n}(x,z) - \overline{S_{m_n}}(z). \tag{3.1}$$

The n subscript refers to a given transect. To compare the fine-scale horizontal variability by transect, we subtract the mean MVBS for the given transect from the S_v for the transect. This results in S_n which is the MVBS anomaly for the given transect. This method is meant to take a closer look at the backscatter variation on different sides of density gradients as well as in relation to the biological and physical parameters captured by the continuous deployment of the EcoCTD.

3.1.2 EcoCTD Parameters

The temperature, salinity, chlorophyll, and oxygen measurements from the EcoCTD are used to compare backscatter at various transects. For consistency, we apply a similar method as in equation 3.1 to calculate the transect anomalies of these parameters using the following equation where χ represents the desired parameter:

$$\chi'(x,z) = \chi_n - \overline{\chi}_m. \tag{3.2}$$

Chlorophyll

The ECOPuck sensor described in section 1.5.1 measures fluorescence in counts which is then converted to chlorophyll-a concentration in $\mu g L^{-1}$ using linear relationships from discrete sampling (Dever et al., 2020). The processed chlorophyll-a concentration is used for this analysis. This transect chlorophyll anomaly calculation is intended to facilitate a closer look at the fine-scale variation of the MVBS in relation to chlorophyll.

Dissolved Oxygen

The Rinko III sensor described in section 1.5.1 determines the oxygen saturation as a percentage for each EcoCTD profile by measuring the phosphorescence life or quenching time of phosphorescence. This is a function of partial pressure in water and high oxygen saturation supports a greater phosphorescence intensity and longer phosphorescence life. Oxygen saturation is a function of temperature, so is computed by the Rinko instrument using its temperature sensor (Dever et al., 2020). Dissolved oxygen (DO) is a measure of how much oxygen is available to living organisms in the water column. DO is a function of absolute salinity, conservative temperature, pressure, and location. It is calculated for the CALYPSO data using the GSW Toolbox in MATLAB (McDougall & Barker, 2011). This is then multiplied by the measured oxygen saturation to get the dissolved oxygen for each EcoCTD profile. The DO anomaly is calculated for each transect using equation

3.2.

Temperature and Salinity

Conservative temperature and absolute salinity (T-S) plots with the total MVBS for the 38kHz and 150kHz ADCPs are plotted at each transect or group of transects to further investigate variations in MVBS. The T-S plots for specific transects do not reveal any horizontal variation patterns, but they provide physical context for the specific transects, especially when considering frontal variations. To get a better idea of how the variations of temperature and salinity with depth might correlate with backscatter, we also apply equation 3.2 to the temperature and salinity.

3.2 Results

Of the 138 transects from February 27 to March 10, 84 had EcoCTD data, they are listed Appendix A. We compare the 38kHz MVBS, 150kHz MVBS, dissolved oxygen, chlorophyll, temperature, and salinity anomalies for each of the 84 transects. The transects are separated into five categories: sunrise (downward migration), sunset (upward migration), daytime, nighttime, and transects with deep chlorophyll intrusions.

A front is defined by a large gradient in one horizontal direction accompanied by a weak one in the perpendicular horizontal direction. In the ocean, fronts are characterized by horizontal density gradients, or sloping isopycnals (McWilliams, 2021). In the analysis of the backscatter anomalies, fronts are identified by density gradients. The frontal variability is assessed for each of the five categories because the characteristics of the backscatter are quite different based on the time of day.

3.2.1 Sunrise/Sunset Transects

Five transects were measured during sunset, which is when upward migration occurs, and four were measured during sunrise, when downward migration occurs.

The downward and upward migration patterns are visible in both the 38kHz and 150kHz MVBS as discussed in section 2.4. S_n is compared with anomalies in DO, chlorophyll, temperature, and salinity, but there is no significant correlation with these physical and biological parameters since the respective migration pattern dominates the backscatter pattern in all cases. Even when there is a strong positive DO anomaly or large shift in temperature and salinity, the backscatter anomaly is not correlated in either the 38kHz or 150kHz MVBS. This demonstrates the importance of the migration patterns of these organisms. It is clear from the sunrise and sunset transects that the biological and physical parameters measured from the EcoCTD do not affect the behavior of the scattering organisms during the migration period. This is consistent with the results from Chapter 2.

3.2.2 Daytime and Nighttime Transects

To understand how biological and physical parameters affect the backscatter measured from the 38kHz and 150kHz ADCPs it is necessary to look more closely at the transects outside of the sunrise/sunset times. This effectively ignores the upward and downward migrations that are shown to take place daily in section 2.4. The total backscatter at night versus during the day is compared for the 38kHz and 150kHz ADCPs by plotting the average MVBS at noon versus midnight for each frequency in Figure 3-1. For the 38kHz ADCP there is a substantial difference in MVBS between noon and midnight for the top 240m with a significantly higher backscatter at midnight as compared to noon. However, for the 150kHz ADCP, the total MVBS is more similar with a slightly higher average MVBS at midnight in the top 100m, but a higher average MVBS for noon from 120m – 200m. This disparity is likely due to the overall stronger return strength in the 38kHz ADCP backscatter as opposed to the 150kHz. In Figure 2-3, the blue bowl-like shape is more distinguishable in the 38kHz MVBS than in the 150kHz MVBS. The daytime and nighttime transects are analyzed separately due to this difference in total average MVBS between noon and midnight and that we expect different organisms to be present during daytime

versus nighttime.

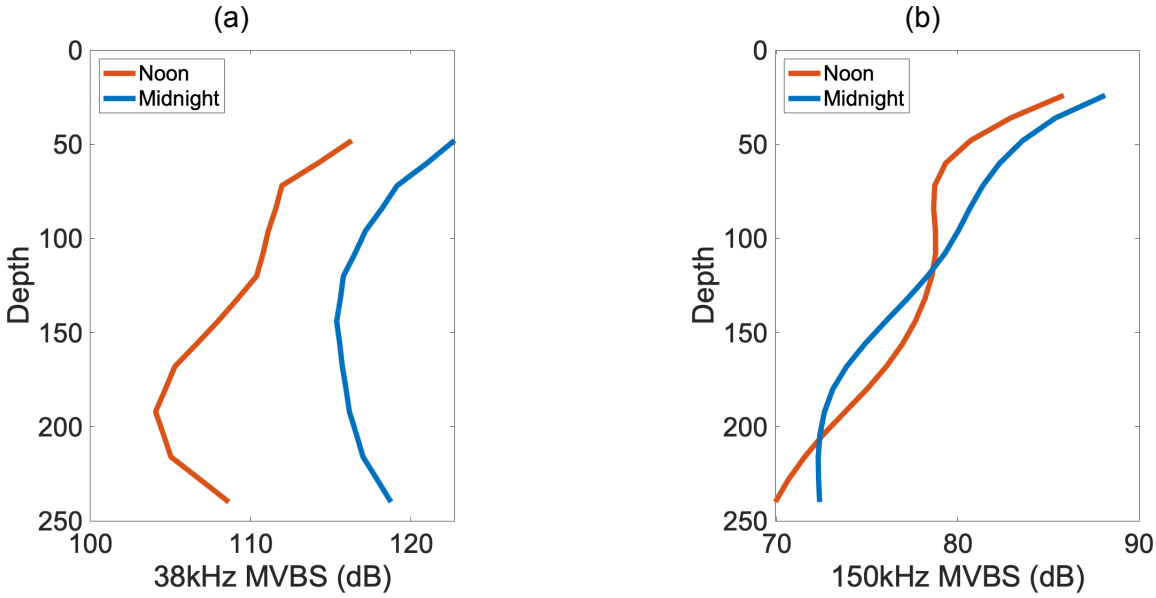

Figure 3-1: The MVBS was averaged for every hour using data from the entire study period. The orange lines are the mean MVBS profile for noon, and the blue lines are the mean profile for midnight. The depth is 240m, which is the maximum sampling depth of the EcoCTD.

Daytime Transects

Transects from five days are evaluated for daytime variability. We chose the transects based on the availability of EcoCTD data and the length of continuous data. In total, 31 individual transects are analyzed and they are grouped together by day so that they covere at least the middle of the day from 11:30-15:45 UTC. The days are March 2, 4, 6, 7, and 8. There is not continuous daytime EcoCTD data on all the days in the 12-day time period due to various operational constraints including equipment malfunction and troubleshooting, deployment and recovery of other instruments such as the WireWalkers, and in some cases hazardous weather.

During all five days, the backscatter anomalies for the 38kHz and 150kHz ADCPs are visually correlated with the DO anomalies. There is very little correlation with chlorophyll, except where chlorophyll is correlated with DO. The temperature and salinity anomalies are inversely correlated with the DO and the backscatter so

high backscatter and high DO are often present in lower salinity and lower temperature waters. In other words, the high backscatter anomalies correlate with higher DO and colder, fresher water. In general, the 38kHz MVBS has a more consistent correlation with the DO.

Each transect has at least one region with sloping isopycnals where the *N/O Pourquoi Pas?* crossed a front. The variability across fronts for each of these days correlates with DO, so if there is high DO on the far side of a front there is also high backscatter. Similarly, when there is low DO at the base of a peak of isopycnals, there are also lower backscatter anomalies. There are a few interesting features in the top 60-70 meters of several of the transects where low backscatter correlated with fresher, colder water but there is not a clear DO anomaly. These spots are likely due to a different water mass signature.

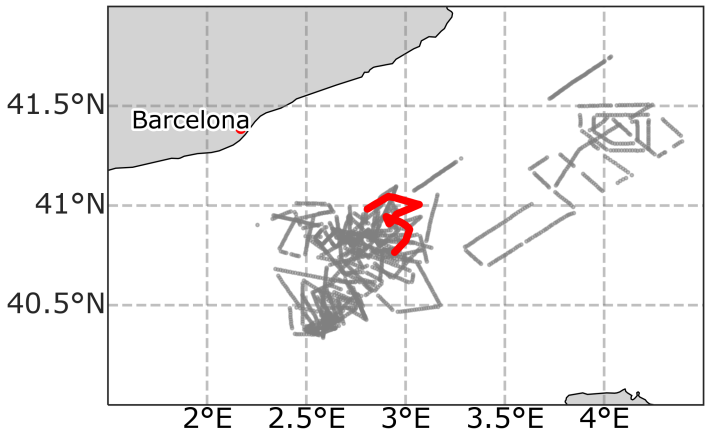

Figure 3-2: Map of all EcoCTD transects with transects 229 – 235 in red. Transects 229 – 235 were measured on March 8 from 08:16 to 15:53 UTC. These daytime transects illustrate the fine-scale variability of the backscatter. Figure courtesy of Kathleen Abbott.

The transects on March 8 (Figure 3-3) highlight the small-scale variability of the backscatter anomaly. It appears that there isn't just one factor that controls where there will be higher backscatter. While higher DO is most often correlated with high backscatter, there is an instance seen in Figure 3-3 where the high backscatter in the 150kHz appears to be aligned with the isopycnals rather than consistent with the biological parameters of DO and chlorophyll. Additionally, the high DO is almost always associated with cooler, fresher water.

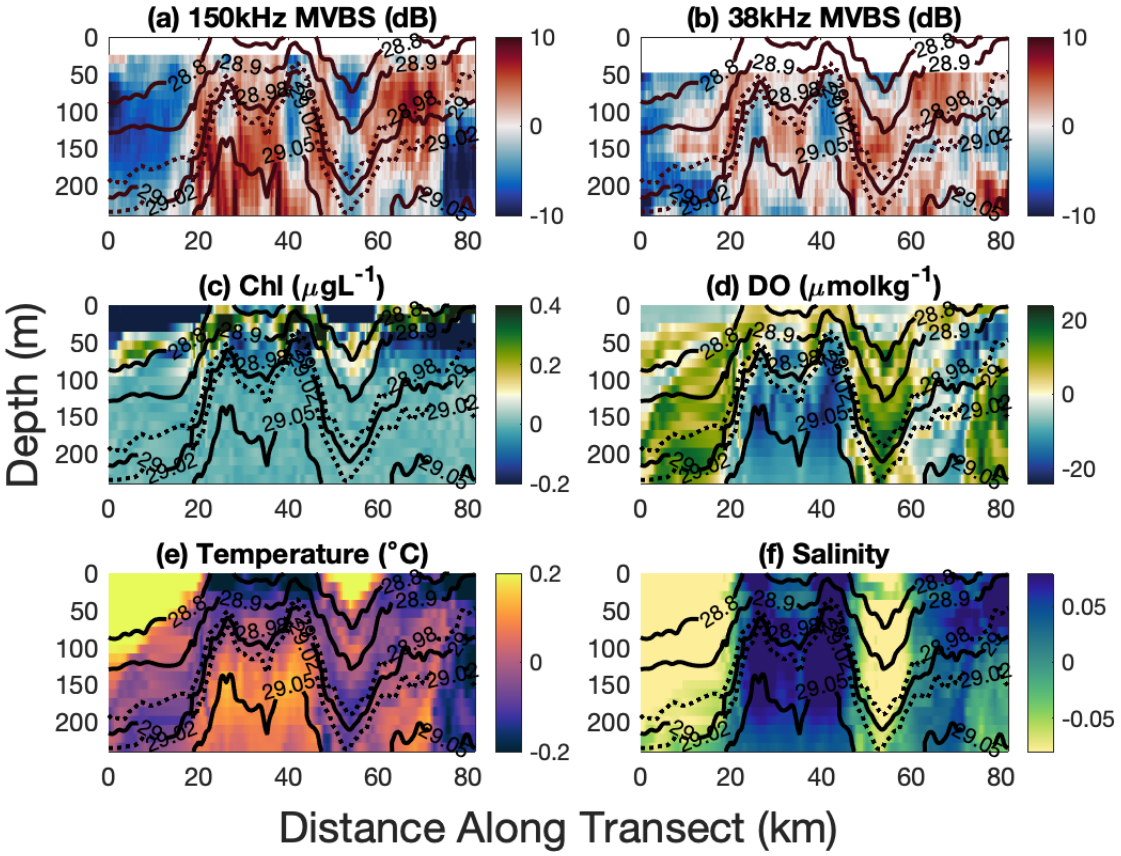

Figure 3-3: Comparisons of MVBS and EcoCTD measurements for transects 229-235 from March 8 from 08:16 to 15:53 UTC. Panels a and b are the 150kHz and 38kHz MVBS transect anomalies, red indicates a positive backscatter anomaly while blue indicates a negative anomaly. Panels c and d are the chlorophyll anomaly and DO anomaly, green is a positive anomaly and blue is a negative anomaly. Panel e is the temperature where the bright yellow and orange signifies warmer water and the blue signifies colder water. Panel f is the salinity anomaly where the blue signifies saltier water and the yellow-green is fresher water.

Nighttime Transects

There are 19 distinct night-time transects of varying length spanning four nights when the ship was navigated to repeatedly survey a cyclonic eddy, and crosses the front that constitutes the periphery. During the 2022 CALYPSO cruise, the CTD casts were almost entirely conducted at night, with each one taking about an hour. This meant that the EcoCTD could not be deployed during that time and there are more gaps in EcoCTD data during the night than the day for this data set. The nights evaluated are March 3, 6, 8, and 9.

Due to DVM, we expect higher overall backscatter to be in the top 240m at night because migrating organisms are closer to the surface to feed at night. This nocturnal DVM pattern is shown to dominate both the 38kHz and 150kHz MVBS in Chapter 2. There is an overall lower correlation between high DO and high backscatter for the nighttime transects as compared to the daytime transects. There is still an inverse correlation between the high temperature and salinity anomalies and the high DO so that the positive DO anomalies are most often present in the colder, fresher water. However, the 38kHz and 150kHz MVBSs do not follow this pattern during the night. This is likely due to the difference in organisms at the surface during the night. As is shown in section 2.4, at night there is a much higher concentration of scatterers in the top 200m in the 38kHz MVBS, and in the top 25m – 80m and 120m – 200m in the 150kHz MVBS. These organisms spend the day time at greater depth, which ostensibly have lower overall DO than the top 200m, it follows that they are less concerned with the level of DO and more concerned with where the most food is. There are a few instances where the backscatter appears to go up and down the isopycnals only, with no other correlation.

The data from March 9 is the most continuous because the *N/O Pourquoi Pas?* and the *R/V Pelagia* conducted a two-ship survey from 20:15 – 06:30 UTC (Figure 3-4). The two-ship survey was intended to sample submesoscale variability in all three dimensions, but the ships ended up cutting through a 30 km eddy for much of the survey. This did provide an interesting comparison across the eddy with the backscatter anomalies. The anticyclonic eddy was cooler, fresher, and lighter, and appears to have trapped a significant amount of DO at least down to 200m (Figure 3-5). There is a corresponding positive anomaly of both 38kHz and 150kHz backscatter in the eddy as well. The 38kHz backscatter anomaly only reaches to about 100m, while the 150kHz backscatter is visible down to 200m. This is likely due to the difference in the sizes of organisms detected by the two different frequencies. The 38kHz backscatter is likely detecting larger, more motile organisms like fish while the 150kHz includes smaller zooplankton. There is also a higher chlorophyll anomaly reaching down to 100m in the eddy. Outside of the eddy, there is not

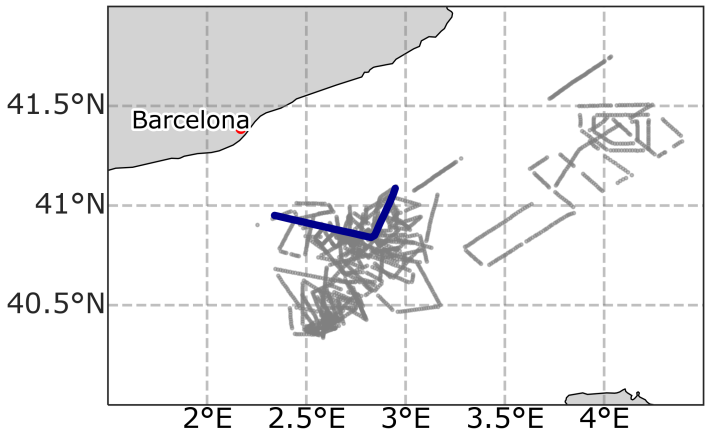

Figure 3-4: Map of all EcoCTD transects with transects 251 – 252 in blue. Transects 251 – 252 were measured on March 9 from 19:28 to 15:19 UTC. These transects are from the two-ship survey at the end of the CALYPSO field campaign where the *N/O Pourquoi Pas* and the *R/V Pelagia* steamed side by side for several hours to collect data to better resolve submesoscale processes. These transects are distinguished by a large anticyclonic eddy that trapped high chlorophyll and DO. Figure courtesy of Kathleen Abbott.

much correlation of backscatter with DO, chlorophyll, or temperature and salinity, which is consistent with the other nighttime transects.

3.2.3 Deep Chlorophyll Intrusions

On February 28 there are three very distinct high chlorophyll and corresponding DO intrusions down to 200m. These intrusions were measured in three separate transects during the day between 11:30 and 17:15 UTC (Figure 3-6). All three features visible in the DO and chlorophyll anomalies have corresponding features in the MVBS for both frequencies (Figure 3-7). The temperature and salinity anomalies for these transects show an inverse relationship where the high backscatter, DO, and chlorophyll correspond to cooler, fresher water. The intrusions cross the isopycnals, which are not sloped, throughout these transects. While this particular analysis does not show how these intrusions got to 200m, the consistency of high backscatter within each intrusion in both the 38kHz and 150kHz MVBS is interesting. The presence of the cooler, fresher water where there is high DO and high chlorophyll suggests that these intrusions have more to do with water mass differ-

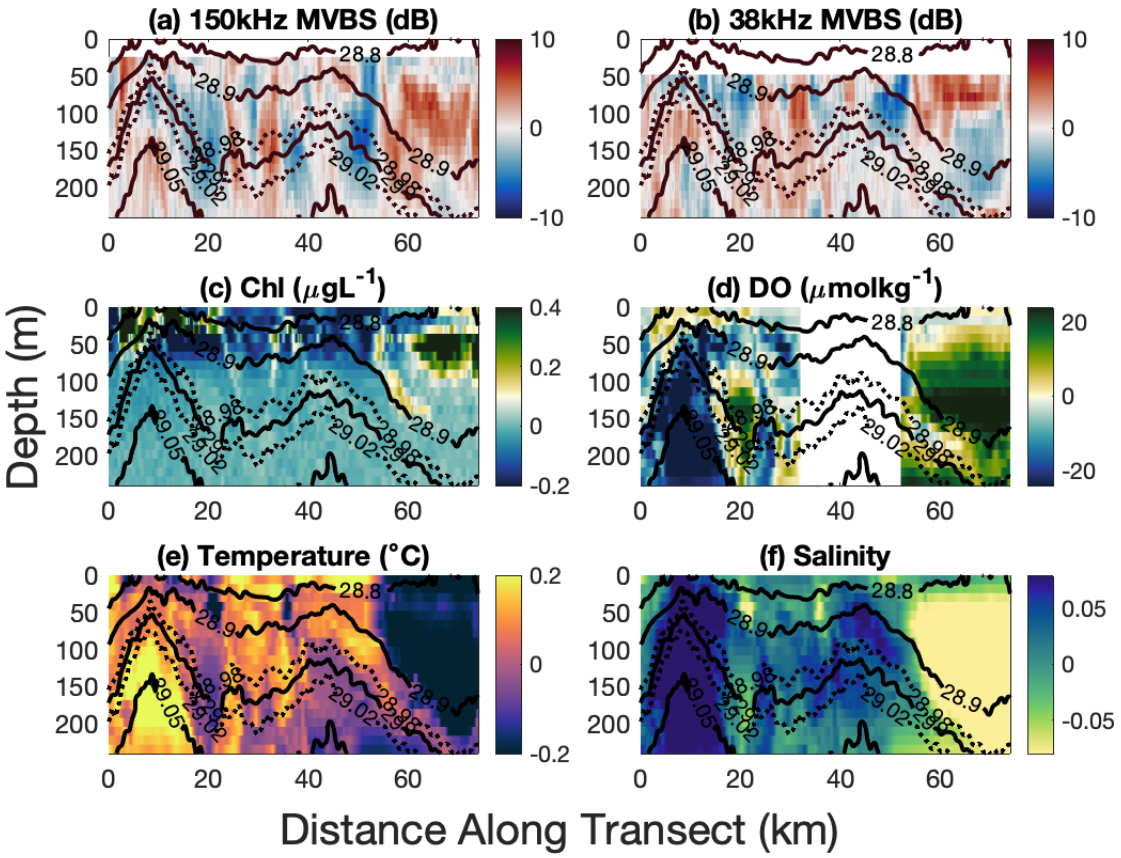

Figure 3-5: Comparisons of MVBS and EcoCTD measurements for transects 251 – 252 from March 9 from 19:28 to 15:19 UTC. Panels a and b are the 150kHz and 38kHz MVBS transect anomalies, red indicates a positive backscatter anomaly while blue indicates a negative anomaly. Panels c and d are the chlorophyll anomaly and DO anomaly, here green is a positive anomaly and blue is a negative anomaly. The missing data in Panel d is due to a faulty oxygen sensor. Panel e is the temperature where the bright yellow and orange signifies warmer water and the blue signifies colder water. Panel f is the salinity anomaly where the blue signifies saltier water and the yellow-green is fresher water. Here, the anticyclonic eddy starts around 60km along the transect and is distinguished by fresh, cold water that has trapped high chlorophyll, high DO, and high backscatter in both the 38kHz and 150kHz MVBS.

ences, but it is difficult to disentangle how long they may have been present since the water appears well stratified in these transects.

3.2.4 Discussion

Comparing the MVBS from the 38kHz and 150kHz ADCPs to temperature, salinity, chlorophyll, and DO requires more fine-scale analysis both at a temporal and

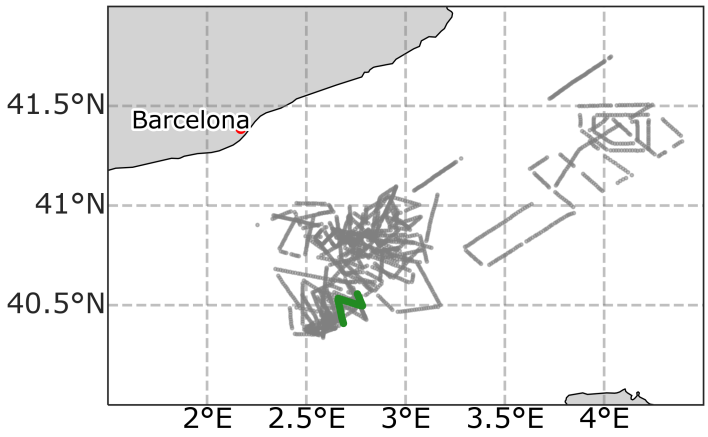

Figure 3-6: Map of all EcoCTD transects with transects 118 – 120. Transects 118 – 120 were measured on February 28 from 13:54 to 17:16 UTC. They are distinguished by deep chlorophyll and DO intrusions reaching to 200m.

length scale. The effects of DVM outweigh any other correlation with biological and physical parameters, requiring a closer look at the transects outside of sunrise and sunset times when vertical migration takes place (as described in Chapter 2).

Since the scattering strength varies between day and night, it is necessary to fine-tune the analysis even more, to evaluate the day and night sections separately. This proves to be interesting, as the MVBS anomalies during the daytime transects correspond well with the DO anomalies in every case with a few notable exceptions. High DO is also usually correlated with fresher, cooler water. However, in the nighttime transects, backscatter shows a lower correlation with DO. Since the migrating organisms in the top 240m of the water column have migrated to the surface to feed at night, it seems likely that they are more concerned with the location of food than DO. It is clear that the backscatter anomalies move up and down with the isopycnals during the night and do not necessarily correspond with the other parameters. Additionally, the backscatter in the top 240m at night would include different organisms (the ones that migrate) than the ones in this area during the day. The migrating organisms may have a lower threshold for the amount of oxygen required for respiration than the organisms that stay in the top 240m during the day.

The case studies of the anticyclonic eddy found during the two-ship survey on

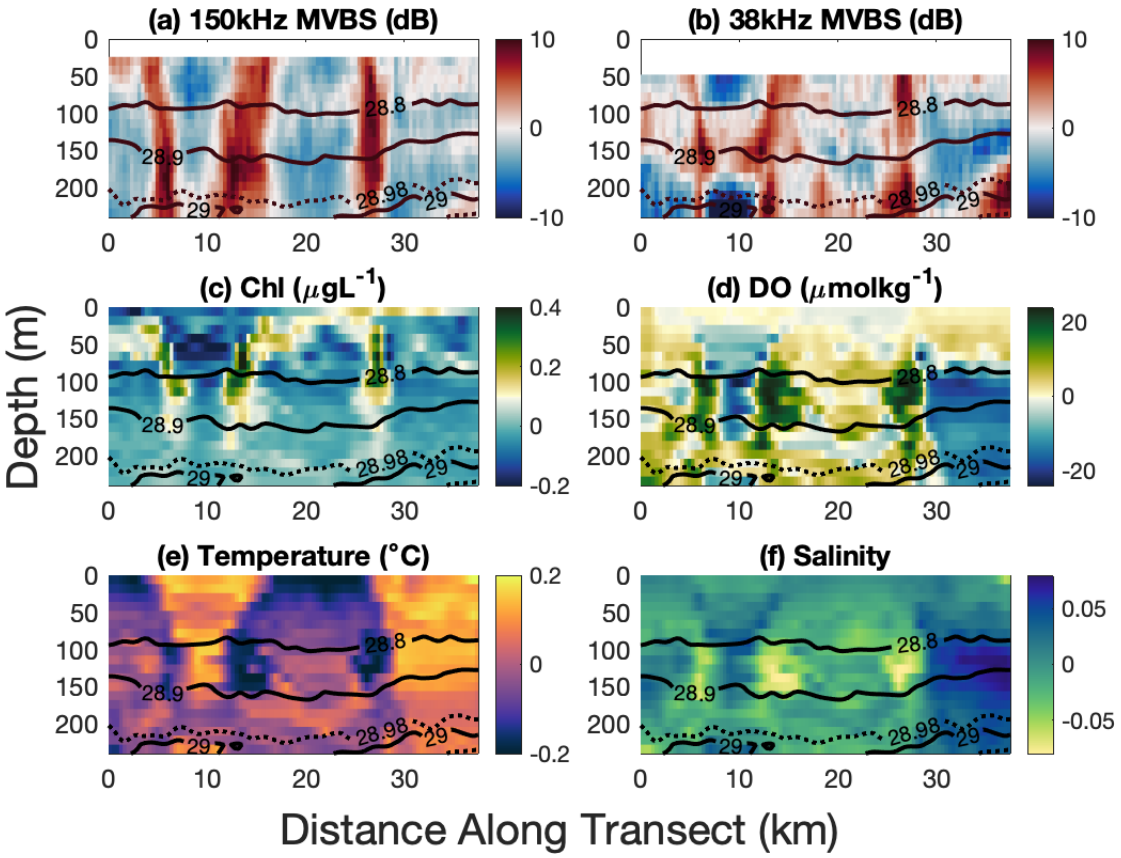

Figure 3-7: Comparisons of MVBS and EcoCTD measurements for transects 118 – 120 from February 28 from 13:54 to 17:16 UTC which are distinguished by deep chlorophyll and DO intrusions. Panels a and b are the 150kHz and 38kHz MVBS transect anomalies respectively, red indicates a positive backscatter anomaly while blue indicates a negative anomaly. Panels c and d are the chlorophyll anomaly and DO anomaly respectively, here green is a positive anomaly and blue is a negative anomaly. The chlorophyll and DO intrusions are visible in green in both panels. Panel e is the temperature where the bright yellow and orange signifies warmer water and the blue signifies colder water. Panel f is the salinity anomaly where the blue signifies saltier water and the yellow-green is fresher water. In this case colder, fresher water correlate with the DO and chlorophyll intrusions which in turn correlate very well with the high backscatter anomalies seen in panels a and b.

March 9 and the three deep chlorophyll intrusions both show a correlation of high backscatter anomaly with high DO and cooler, fresher water. The correlations observed in these case studies are consistent with the daytime transects. The transects with the chlorophyll intrusions were measured during the day, and consistent with the other daytime transects, MVBS was correlated with the DO in every part of the transect. However, the eddy was measured during the night, and the eddy

was the only part of the transect where MVBS correlated with the DO. The other backscatter anomalies did not seem to correlate with the EcoCTD parameters.

Overall, migration and the presence of higher scatterers during the night had the strongest impact on the pattern of backscatter in the 150kHz and 38kHz ADCP data. However, when DVM is not the major factor, DO has the strongest impact on where the most scatterers are present, as shown in both the 38kHz and 150kHz ADCP data.

Chapter 4

Concluding Remarks

4.1 Author's Note

I had the tremendous opportunity to collect the data used in this thesis as a member of the science party onboard the *N/O Pourquoi Pas?* during the CALYPSO 2022 Field Campaign. The large and diverse data set we collected in the Balearic Sea is unique in its breadth and detail, as we collected physical and biological data spanning a range of projects. We deployed hundreds of drifters, used multiple types of floats, continuously collected data using the ship's instruments including ADCPs and the meteorological instrument suite, collected almost 3,000 EcoCTD profiles – the most on any cruise at that time – and collected water samples for multiple biological experiments and studies, including work on microplastics in the region. The CALYPSO goal to diagnose vertical pathways led us to extensively sample intriguing submesoscale phenomena including an area of deep convection, and two cyclonic eddies, one of which elongated into a ridge and then collapsed into two smaller eddies. The adaptive sampling technique we used made the cruise dynamic and interesting. I personally spent many long hours deploying the EcoCTD, and am thrilled to have had the opportunity to analyze this data myself as part of my thesis.

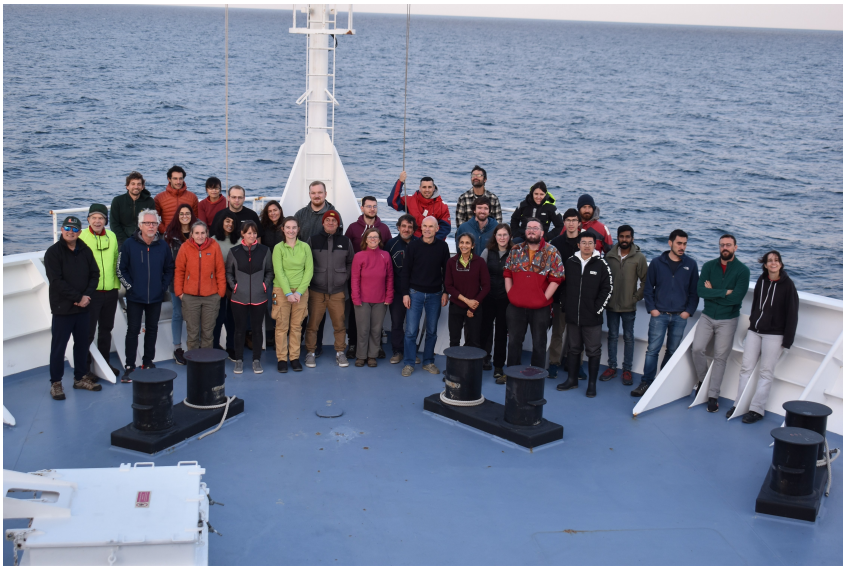

Figure 4-1: The science party on the bow of the *N/O Pourquoi Pas?*.

4.2 Summary

In this thesis, I first characterize the SSLs in the Balearic Sea using ADCP backscatter and then compare the backscatter to biological and physical measurements from the EcoCTD. We apply the sonar equation to the raw echo intensity data to calculate the MVBS, which is used to illustrate the scattering layers. Due to the difference in frequencies, we expect the 38kHz ADCP to detect larger organisms on the 1 – 2cm scale while the 150kHz ADCP is expected to detect zooplankton on the 2.5 – 5mm scale (see Table 1.2). From the 38kHz daily composite, S_D, and MVBS anomaly, S_0, we find that there is a permanent scattering layer from 300m – 500m and two migrating layers, one in the top 50m and one that migrates from 150m – 250m to 350m – 600m. In the 150kHz ADCP, there is a permanent scattering layer from 350m – 440m and two distinct migrating layers in the S_D that are more distinguishable than in the 38kHz MVBS, this is likely due to the higher resolution of the 150kHz ADCP. The first layer spends the night in the top 50m and descends to 75m – 120m during the day. The second spends the night between 120m – 200m and migrates to about 300m during the day.

The swimming speeds are found to be 2 – 11cms^{-1} in the 38kHz MVBS, which

is consistent with previous work in this region (Tarling et al., 2001). However, the speeds for the 150kHz MVBS are generally lower, at 1 – 2cms^{-1}. This disparity is unexpected as previous studies in this region used 150kHz ADCPs. This could be due to differences in the two ADCPs used on the *N/O Pourquoi Pas?*. The backscatter from the 38kHz ADCP is very strong and DVM patterns are immediately visible, the extraction of migrating layers is straightforward, and because of the depth range of the instrument, the full slope of vertical migration is visible for both the ascent and descent migrations. For the 150kHz ADCP, the DVM pattern is weaker and the vertical migration slopes are not as well defined in S_0.

Based on previous studies and the ADCP frequencies, the organisms constituting the scattering signal are likely krill and pteropods for the 150kHz ADCP, and larger pteropods and fish for the 38kHz ADCP. It is interesting that the DVM in the 38kHz ADCP is relatively stronger than the 150kHz ADCP. This could mean that there are more pelagic fish and large pteropods migrating. It is also reasonable that these larger organisms may have a stronger return than the smaller zooplankton, especially if they have gas inclusions such as swimbladders as many species of pelagic fish. Modeling the subsurface light shows that the upward and downward migrations follow the isolumes. There is also evidence of small changes in the isolume depths during the day resulting in an adjustment of the organisms. During the daytime, the organisms at depth are clearly found along isopycnals.

In Chapter 3, we use the EcoCTD data to compare backscatter with biological and physical parameters to better understand backscatter variability in relation to fronts. We find that it was necessary to divide the transects with EcoCTD and ADCP data into groups based on the time of day because of the overwhelmingly dominant effect of DVM. During sunrise and sunset, when downward or upward migration is occurring, the backscatter does not correlate with any of the EcoCTD measurements. We divide the transects into daytime and nighttime and compare those to the temperature, salinity, chlorophyll concentration, and DO in the top 240m from the EcoCTD. The backscatter in the daytime transects, when migrating organisms are at depth, had high positive anomaly correlations with the positive anomalies of

Figure 4-2: The author on EcoCTD watch with Dr. Alex Kinsella on the stern of the *N/O Pourquoi Pas?* with the EcoCTD on deck.

DO in every case. For the nighttime transects, the high backscatter anomalies often correlate somewhat with the DO but not as closely as the daytime transects. Since the migrating organisms have migrated to the surface to feed at night we hypothesize that they are likely more interested in food and are not limited by DO at these depths. There are a few transects with deep DO and chlorophyll intrusions which correlate well with high backscatter anomalies in both frequencies. At frontal areas or intrusions where there is high DO and chlorophyll that may have been trapped by submesoscale processes, there is also high backscatter. In almost every instance, high DO also correlates with fresher, colder water indicating that there is likely a water mass origin element to the presence of backscatter.

4.3 Discussion

The finding that high backscatter is most consistently correlated with high DO is consistent with previous findings. In a 2013 study using a global array of ADCP backscatter data from 1990 – 2011, Bianchi et al. found that the best single predictor of migration depth for organisms that practice DVM is seawater oxygen con-

centration. Globally, the migration depth is greater where the subsurface oxygen concentrations are high. In oxygen minimum zones the migratory animals descend as far as the upper margins of the low-oxygen areas (Bianchi et al., 2013). A study in the eastern tropical North Pacific, a major oceanic oxygen minimum zone (OMZ), found that very small differences in oxygen ($\sim 3\mu$M) had a significant effect on zooplankton in the region (Wishner et al., 2018).

Many marine animals rely on sound to navigate, communicate, and feed, and some are very sensitive to underwater sounds. Anthropogenic underwater noise has been shown to adversely affect many species of marine animals from whales and dolphins to zooplankton (McCauley et al., 2017). Since Naval sonar was linked to the mass stranding of beaked whales in the Bahamas in 2000, the Navy and many other funding sources have invested significantly in research to understand the effects of underwater sound on marine animals at all trophic levels of the food web (Balcomb III & Claridge, 2001). With the increased commercial and government interest in building offshore wind farms, studies of the effects of sound include not just active sonar, but also the noise from various types of drilling and hammering into the seabed. These types of sounds have even been shown to change the behavior of bivalves like the giant scallop (Jézéquel et al., 2022).

Since ADCPs are active acoustic instruments, there is concern that the sound pings may adversely affect the organisms in the water column. In general, the low power output of ADCPs and short pulse lengths are considered to be safe for marine animals. A cruise in the Eastern Tropical Pacific which had marine mammal observers onboard found that baleen whales had no significant responses to ADCPs while spotted and spinner dolphins were detected slightly more often and beaked whales less often when ADCPs were transmitting (Gerrodette & Pettis, 2005). It is difficult to find much research on the effects of ADCPs specifically on marine animals. In comparison to ADCPs, echosounders and sonars have higher power outputs and are generally more concerning. Another important note is that it is extremely difficult to study the effects of noise on most marine animals; while the body of literature continues to grow, most studies are extremely situation and species-

specific. Even for marine mammals, by far the most studied animals in this area, the sample sizes are small and results could be limited to the nuanced behaviors of an individual whale or dolphin. It is widely assumed that the sound emitted from ADCPs has a minimal effect on marine animals. Nonetheless, it is still important to consider the potential impacts of transmitting sound on the ecosystem.

Using acoustic backscatter, technically a byproduct of ADCPs, to characterize biological scatterers in the water column is not a novel concept. Many studies using acoustic backscatter have also used net tows, such as MOCNESS, to quantify the abundance of zooplankton and identify the taxonomy. We did not collect net tows during the CALYSPO cruise as the primary objective was physical oceanographic data collection, so we did not attempt to quantify or identify which organisms were detected by the ADCPs. However, we successfully characterized the SSLs with the existing data set and were able to compare backscatter anomalies with biological and physical measurements. ADCPs are ubiquitous on oceanographic research vessels for collecting current velocity measurements and they all also collect echo intensity. There is a vast cache of this data available, and it can be used to identify DVM patterns and migration depths and velocities on a global scale as demonstrated by Bianchi et al., 2013 and Bianchi and Mislan, 2016. While useful for establishing global trends, this available data can also be used to characterize regional SSLs. Due to the significant impact of migrating organisms on the global carbon cycle, it is important to obtain a better understanding of how SSLs may have changed using historical data that could be revealing about the effects of climate change. Additionally, understanding where to expect SSLs in the open ocean would assist in navigation for submarines.

While acoustic measurements are useful, especially when so many ADCP backscatter measurements all over the globe already exist, they do not allow us to identify individual or aggregate organisms through ADCP or echosounder data alone. There is a vast collection of literature in bioacoustics working to model various organisms from fish to hard-shelled and gelatinous zooplankton so that echo sounders can be used to characterize fish stocks. However, with small organisms like zooplank-

ton that do not have gas inclusions, ADCP and echosounder data is limited even with modeling. While net tows fill in some gaps, there are concerns about avoidance behavior when using nets. Recent developments in in-situ imaging systems for studying plankton include profiling optical instruments like stereo cameras and In-Situ Ichthyoplankton Imaging System Technology (ISIIS) that use shadowgraph imaging to sample a large volume of water at high speed for zooplankton ecology. The imaging records taxonomic and behavioral information at fine scales without the bias against gelatinous organisms associated with net tows (Grassian et al., 2023). This development produces thousands of images that need to be sorted either by hand or through machine learning.

ADCP data is not available in every part of the world as some oceans are sampled significantly more than others. Climate and biogeochemical models require a full global picture of DVM as it is an essential part of the global carbon cycle. Global studies using ADCP data have shown that DVM patterns vary based on longitude, for example, vertical velocities of migrators are highest in tropical and subtropical regions and decline towards the poles (Bianchi & Mislan, 2016). Some of these gaps in understanding global DVM can be filled through the use of remote sensing. A satellite-mounted light-detection-and-ranging (lidar) instrument that collects optical signals from DVM animals that migrate to the surface at night was used to describe global patterns of DVM in ocean animals (Behrenfeld et al., 2019). The use of remote sensing in concert with more fine-scale sampling could yield interesting results and contribute to our understanding of DVM.

Characterizing the patterns of DVM has been approached from small scales with data from individual ships like in this thesis, all the way up to global patterns of DVM using data collected from space. The vast literature and diversity of approaches taken towards understanding, characterizing, and parameterizing DVM demonstrates its importance. Not only is it the most impressive migration of organisms on Earth, but it is also essential to the global carbon cycle, something that only becomes more urgent to understand as we search for solutions to the climate crisis.

Bibliography

Archibald, K. M., Siegel, D. A., & Doney, S. C. (2019). Modeling the impact of zooplankton diel vertical migration on the carbon export flux of the biological pump. *Global Biogeochemical Cycles*, *33*(2), 181–199.

Ashjian, C. J., Smith, S. L., Flagg, C. N., & Wilson, C. (1998). Patterns and occurrence of diel vertical migration of zooplankton biomass in the Mid-Atlantic Bight described by an acoustic Doppler current profiler. *Continental Shelf Research*, *18*(8), 831–858.

Balcomb III, K. C., & Claridge, D. E. (2001). A mass stranding of cetaceans caused by naval sonar in the bahamas. *Bahamas journal of science*, *8*(2), 2–12.

Bayly, I. (1986). Aspects of diel vertical migration in zooplankton, and its enigma variations. In *Limnology in australia* (pp. 349–368). Springer.

Beauducel, F. (2023). Sunrise: Sunrise and sunset times (https://github.com/beaudu/sunrise/releases/tag/v1.4.1). *GitHub*, Retrieved 2/24/2023.

Behrenfeld, M. J., Gaube, P., Della Penna, A., O'malley, R. T., Burt, W. J., Hu, Y., Bontempi, P. S., Steinberg, D. K., Boss, E. S., Siegel, D. A., et al. (2019). Global satellite-observed daily vertical migrations of ocean animals. *Nature*, *576*(7786), 257–261.

Berge, J., Cottier, F., Varpe, Ø., Renaud, P. E., Falk-Petersen, S., Kwasniewski, S., Griffiths, C., Søreide, J. E., Johnsen, G., Aubert, A., et al. (2014). Arctic complexity: A case study on diel vertical migration of zooplankton. *Journal of Plankton Research*, *36*(5), 1279–1297.

Bianchi, D., Galbraith, E. D., Carozza, D. A., Mislan, K., & Stock, C. A. (2013). Intensification of open-ocean oxygen depletion by vertically migrating animals. *Nature Geoscience*, *6*(7), 545–548.

Bianchi, D., & Mislan, K. (2016). Global patterns of diel vertical migration times and velocities from acoustic data. *Limnology and Oceanography*, *61*(1), 353–364.

Bozzano, R., Fanelli, E., Pensieri, S., Picco, P., & Schiano, M. (2014). Temporal variations of zooplankton biomass in the Ligurian Sea inferred from long time series of ADCP data. *Ocean Science*, *10*(1), 93–105.

Brierley, A. S. (2014). Diel vertical migration. *Current biology*, *24*(22), R1074–R1076.

Cisewski, B., & Strass, V. H. (2016). Acoustic insights into the zooplankton dynamics of the eastern Weddell Sea. *Progress in Oceanography*, *144*, 62–92.

Cisewski, B., Strass, V. H., Rhein, M., & Krägefsky, S. (2010). Seasonal variation of diel vertical migration of zooplankton from ADCP backscatter time series data in the Lazarev Sea, Antarctica. *Deep Sea Research Part I: Oceanographic Research Papers*, *57*(1), 78–94.

Cohen, J. H., & Forward Jr, R. B. (2002). Spectral sensitivity of vertically migrating marine copepods. *The Biological Bulletin*, *203*(3), 307–314.

Deines, K. L. (1999). Backscatter estimation using broadband acoustic Doppler current profilers. *Proceedings of the IEEE Sixth Working Conference on Current Measurement (Cat. No. 99CH36331)*, 249–253.

Dever, M., Freilich, M., Farrar, J. T., Hodges, B., Lanagan, T., Baron, A. J., & Mahadevan, A. (2020). EcoCTD for profiling oceanic physical–biological properties from an underway ship. *Journal of Atmospheric and Oceanic Technology*, *37*(5), 825–840.

Dozier, J. (2023). Sunposition (https://www.mathworks.com/matlabcentral/file exchange/ 74939-sun-position). *MATLAB Central File Exchange*, Retrieved 5/11/2023.

Fernández de Puelles, M. L., Valencia, J., & Vicente, L. (2004). Zooplankton variability and climatic anomalies from 1994 to 2001 in the Balearic Sea (Western Mediterranean). *ICES Journal of Marine Science*, *61*(4), 492–500.

Fernández de Puelles, M. L., Alemany, F., & Jansá, J. (2007). Zooplankton time-series in the Balearic Sea (Western Mediterranean): Variability during the decade 1994–2003. *Progress in Oceanography*, *74*(2-3), 329–354.

Flagg, C. N., & Smith, S. L. (1989). On the use of the acoustic Doppler current profiler to measure zooplankton abundance. *Deep Sea Research Part A. Oceanographic Research Papers*, *36*(3), 455–474.

Francois, R., & Garrison, G. (1982a). Sound absorption based on ocean measurements: Part I: Pure water and magnesium sulfate contributions. *The Journal of the Acoustical Society of America*, *72*(3), 896–907.

Francois, R., & Garrison, G. (1982b). Sound absorption based on ocean measurements. part II: Boric acid contribution and equation for total absorption. *The Journal of the Acoustical Society of America*, *72*(6), 1879–1890.

Freilich, M. (2018). Forecasting where ocean life thrives: Scientists focus on seams in the ocean called'fronts'. *Oceanus*, *53*(2), 20–24.

Freilich, M., & Mahadevan, A. (2019). Decomposition of vertical velocity for nutrient transport in the upper ocean. *Journal of Physical Oceanography*, *49*(6), 1561–1575.

Freilich, M., & Mahadevan, A. (2021). Coherent pathways for subduction from the surface mixed layer at ocean fronts. *Journal of Geophysical Research: Oceans*, *126*(5), e2020JC017042.

Garcia, E., Tintoré, J., Pinot, J. M., Font, J., & Manriquez, M. (1994). Surface circulation and dynamics of the Balearic Sea. *Seasonal and Interannual variability of the Western Mediterranean Sea*, *46*, 73–91.

Gerrodette, T., & Pettis, J. (2005). Responses of tropical cetaceans to an echosounder during research vessel surveys. *Abstr. 16th Bien. Conf. Biol. Mar. Mamm.*, 104.

Goffredo, S., & Dubinsky, Z. (2013). *The Mediterranean Sea: Its history and present challenges*. Springer Science & Business Media.

Gordon, R. L., & Instruments, R. (2011). Acoustic Doppler current profiler: Principles of operation: A practical primer. *RD Instruments, San Diego*.

Gostiaux, L., & van Haren, H. (2010). Extracting meaningful information from uncalibrated backscattered echo intensity data. *Journal of Atmospheric and Oceanic Technology*, *27*(5), 943–949.

Grassian, B., Roman, C., Omand, M., Wishner, K., & Seibel, B. (2023). Multi-sensor observation of a rapidly dispersing micronekton thin layer. *Deep Sea Research Part I: Oceanographic Research Papers*, *191*, 103924.

Greene, C. (2023). Pathdist (https://www.mathworks.com/matlabcentral/file exchange/47042pathdist). *MATLAB Central File Exchange*, Retrieved 8/3/2023.

Heywood, K. J., Scrope-Howe, S., & Barton, E. (1991). Estimation of zooplankton abundance from shipborne ADCP backscatter. *Deep Sea Research Part A. Oceanographic Research Papers*, *38*(6), 677–691.

Jézéquel, Y., Cones, S., Jensen, F. H., Brewer, H., Collins, J., & Mooney, T. A. (2022). Pile driving repeatedly impacts the giant scallop (*Placopecten magellanicus*). *Scientific reports*, *12*(1), 15380.

Liu, Y., Guo, J., Xue, Y., Sangmanee, C., Wang, H., Zhao, C., Khokiattiwong, S., & Yu, W. (2022). Seasonal variation in diel vertical migration of zooplankton and micronekton in the Andaman Sea observed by a moored ADCP. *Deep Sea Research Part I: Oceanographic Research Papers*, *179*, 103663.

Mahadevan, A., Pascual, A., Rudnick, D. L., Ruiz, S., Tintoré, J., & D'Asaro, E. (2020). Coherent pathways for vertical transport from the surface ocean to interior. *Bulletin of the American Meteorological Society*, *101*(11), E1996–E2004.

McCauley, R. D., Day, R. D., Swadling, K. M., Fitzgibbon, Q. P., Watson, R. A., & Semmens, J. M. (2017). Widely used marine seismic survey air gun operations negatively impact zooplankton. *Nature ecology & evolution*, *1*(7), 0195.

McDougall, T. J., & Barker, P. M. (2011). Getting started with TEOS-10 and the Gibbs Seawater (GSW) oceanographic toolbox. *Scor/Iapso WG*, *127*(532), 1–28.

McWilliams, J. C. (2021). Oceanic frontogenesis. *Annual Review of Marine Science*, *13*, 227–253.

Middleton, L. (2023). Calypso 2022 data report. *Manuscript in preparation*.

Molinero, J. C., Ibanez, F., Souissi, S., Bosc, E., & Nival, P. (2008). Surface patterns of zooplankton spatial variability detected by high frequency sampling in the NW Mediterranean. role of density fronts. *Journal of Marine Systems*, *69*(3-4), 271–282.

Mullison, J. (2017). Backscatter estimation using broadband acoustic Doppler current profilers-updated. *Proceedings of the ASCE Hydraulic Measurements & Experimental Methods Conference, Durham, NH, USA*, 9–12.

Omand, M. M., Steinberg, D. K., & Stamieszkin, K. (2021). Cloud shadows drive vertical migrations of deep-dwelling marine life. *Proceedings of the National Academy of Sciences*, *118*(32), e2022977118.

Peña, M., Olivar, M. P., Balbín, R., López-Jurado, J. L., Iglesias, M., & Miquel, J. (2014). Acoustic detection of mesopelagic fishes in scattering layers of the Balearic Sea (western Mediterranean). *Canadian Journal of Fisheries and Aquatic Sciences*, *71*(8), 1186–1197.

Pinkel, R., Goldin, M., Smith, J., Sun, O., Aja, A., Bui, M., & Hughen, T. (2011). The WireWalker: A vertically profiling instrument carrier powered by ocean waves. *Journal of Atmospheric and Oceanic Technology*, *28*(3), 426–435.

Pinot, J. M., & Jansá, J. (2001). Time variability of acoustic backscatter from zooplankton in the Ibiza Channel (western Mediterranean). *Deep Sea Research Part I: Oceanographic Research Papers*, *48*(7), 1651–1670.

Plueddemann, A. J., & Pinkel, R. (1989). Characterization of the patterns of diel migration using a Doppler sonar. *Deep Sea Research Part A. Oceanographic Research Papers*, *36*(4), 509–530.

Proud, R., Cox, M. J., Wotherspoon, S., & Brierley, A. S. (2015). A method for identifying sound scattering layers and extracting key characteristics. *Methods in Ecology and Evolution*, *6*(10), 1190–1198.

Schroeder, K., & Chiggiato, J. (2022). *Oceanography of the Mediterranean Sea: An introductory guide*. Elsevier.

Steinberg, D. K., & Landry, M. R. (2017). Zooplankton and the ocean carbon cycle. *Annual review of marine science*, *9*, 413–444.

Tarling, G. A., Matthews, J., David, P., Guerin, O., & Buchholz, F. (2001). The swarm dynamics of northern krill (*Meganyctiphanes norvegica*) and pteropods (Cavolinia inflexa) during vertical migration in the Ligurian Sea observed by an acoustic doppler current profiler. *Deep Sea Research Part I: Oceanographic Research Papers*, *48*(7), 1671–1686.

Urick, J., Robert. (1983). *Principles of underwater sound*. McGraw-Hill Book Company.

Wilson, T., Lwiza, K. M., & Allen, G. L. (1997). Performance comparison of RDI ADCPs: Broadband versus narrowband. *Oceans' 97. MTS/IEEE Conference Proceedings*, *1*, 120–125.

Wishner, K. F., Seibel, B. A., Roman, C., Deutsch, C., Outram, D., Shaw, C. T., Birk, M. A., Mislan, K., Adams, T., Moore, D., et al. (2018). Ocean deoxygenation and zooplankton: Very small oxygen differences matter. *Science advances*, *4*(12), eaau5180.

Woodward, W., & Appell, G. (1986). Current velocity measurements using acoustic Doppler backscatter: A review. *IEEE Journal of oceanic engineering*, *11*(1), 3–6.

Yang, C., Xu, D., Chen, Z., Wang, J., Xu, M., Yuan, Y., & Zhou, M. (2019). Diel vertical migration of zooplankton and micronekton on the northern slope of the South China Sea observed by a moored ADCP. *Deep Sea Research Part II: Topical Studies in Oceanography*, *167*, 93–104.

Zheng, B., Lucas, A., Franks, P., Schlosser, T., C.R., A., Send, U., Davis, K., Barton, A., & Sosik, H. (2023). Dinoflagellate vertical migration fuels an intense red

tide. *Proceedings of the National Academy of Sciences of the United States of America*, Accepted.

Appendix A

Transects used in Chapter 3

Transect	Initial Lat	Initial Lon	Final Lat	Final Lon	Start	End	Time of Day
117	40.4198	2.6087	40.558	2.7524	2/28 11:31	2/28 13:41	Day
118	40.5574	2.7558	40.4935	2.7838	2/28 13:54	2/28 14:35	Day
119	40.4961	2.7783	40.5337	2.6601	2/28 14:47	2/28 15:43	Day
120	40.5319	2.658	40.3996	2.6885	2/28 15:54	2/28 17:16	Day
121	40.3964	2.682	40.3778	2.4869	2/28 17:21	2/28 19:35	Sunset
127	40.3347	2.5792	40.4012	2.5851	3/1 07:39	3/1 08:32	Sunrise
144	40.8928	2.9788	40.7421	2.8086	3/2 09:15	3/2 11:42	Day
145	40.7391	2.7947	40.7909	2.686	3/2 11:51	3/2 12:54	Day
146	40.7967	2.685	40.8694	2.7365	3/2 12:58	3/2 13:53	Day
147	40.8715	2.7413	40.7642	2.9894	3/2 13:57	3/2 16:02	Day
148	40.7569	2.9934	40.7002	2.9876	3/2 16:08	3/2 16:43	Day
149	40.7068	2.9769	40.8641	2.6366	3/2 16:54	3/2 20:09	Sunset
155	40.7269	2.6705	40.8068	2.765	3/3 10:30	3/3 11:41	Day
161	40.8141	2.8976	40.8663	2.7859	3/3 17:41	3/3 18:42	Sunset
162	40.8674	2.7993	40.8771	2.9445	3/3 18:55	3/3 20:04	Night
163	40.8802	2.9489	40.9882	2.9584	3/3 20:08	3/3 21:12	Night
169	40.9068	2.796	40.9997	2.8017	3/4 02:29	3/4 03:29	Night
172	40.7339	2.9488	40.7129	3.1018	3/4 11:34	3/4 12:42	Day
173	40.7217	3.1048	40.8507	3.0713	3/4 12:48	3/4 14:02	Day
174	40.8567	3.0634	40.8101	2.8519	3/4 14:08	3/4 15:51	Day
176	40.8135	3.0244	40.8463	2.4968	3/4 18:03	3/5 01:15	Night
177	40.839	2.5003	40.7591	2.6132	3/5 01:26	3/5 02:31	Night
181	41.0126	2.4457	41.0093	2.6047	3/5 15:01	3/5 16:23	Day
182	40.9712	2.6204	40.9341	2.4591	3/5 16:59	3/5 18:19	Sunset
183	40.93	2.4564	40.8894	2.4723	3/5 18:32	3/5 18:59	Sunset
184	40.8875	2.4848	40.9145	2.6103	3/5 20:02	3/5 21:06	Night
185	40.9097	2.6184	40.8382	2.6507	3/5 21:59	3/5 22:44	Night

186	40.8353	2.6553	40.8708	2.736	3/5 22:48	3/5 23:33	Night
187	40.865	2.7367	40.7306	2.7308	3/6 00:32	3/6 01:53	Night
188	40.7199	2.731	40.7988	2.8076	3/6 02:04	3/6 03:00	Night
189	40.7988	2.8169	40.7381	2.8655	3/6 03:05	3/6 03:48	Night
190	40.7363	2.8742	40.7835	3.1168	3/6 03:52	3/6 05:47	Night
191	40.7888	3.1262	40.8402	2.9442	3/6 05:58	3/6 07:31	Sunrise
194	40.8539	2.9968	40.8502	2.7892	3/6 09:06	3/6 10:46	Day
195	40.8737	2.7733	40.8097	2.7421	3/6 11:09	3/6 11:59	Day
196	40.8072	2.738	40.8267	2.6701	3/6 12:13	3/6 12:48	Day
197	40.8338	2.6731	40.967	2.7227	3/6 12:54	3/6 14:23	Day
198	40.9681	2.7319	40.899	2.8266	3/6 14:28	3/6 15:30	Day
199	40.9017	2.8314	40.9818	2.9254	3/6 15:34	3/6 16:43	Day
200	40.9811	2.9281	40.9106	2.9594	3/6 16:54	3/6 17:41	Sunset
201	40.9091	2.9639	40.9487	3.0825	3/6 17:54	3/6 18:56	Sunset
202	40.9443	3.0774	40.8708	2.9922	3/6 19:05	3/6 20:09	Night
203	40.8844	2.9912	40.8928	2.912	3/6 21:19	3/6 21:55	Night
207	40.9753	2.9491	41.0519	2.9134	3/7 01:16	3/7 02:03	Night
208	41.0481	2.9085	40.7921	2.6471	3/7 02:09	3/7 07:52	Night
209	40.7928	2.642	40.8858	2.5826	3/7 07:56	3/7 08:59	Sunrise
210	40.8856	2.5812	40.8376	2.5426	3/7 09:05	3/7 09:38	Day
211	40.8316	2.5433	40.8046	2.5747	3/7 09:42	3/7 10:04	Day
212	40.807	2.5814	40.8848	2.657	3/7 10:10	3/7 11:12	Day
213	40.8815	2.6622	40.7962	2.7283	3/7 11:17	3/7 12:19	Day
214	40.7961	2.7355	40.8816	2.8111	3/7 12:23	3/7 13:21	Day
215	40.8742	2.8151	40.7995	2.8645	3/7 13:30	3/7 14:18	Day
216	40.7959	2.8703	40.838	2.9068	3/7 14:23	3/7 14:51	Day
217	40.8417	2.9067	40.8744	2.8766	3/7 14:54	3/7 15:17	Day
218	40.8708	2.8775	40.7912	2.8089	3/7 15:27	3/7 16:28	Day
219	40.792	2.8034	40.8709	2.74	3/7 16:31	3/7 17:26	Day
220	40.8714	2.7339	40.7948	2.6496	3/7 17:30	3/7 18:30	Sunset
222	40.8817	2.5795	40.8362	2.5404	3/7 20:25	3/7 21:02	Night
223	40.8305	2.5421	40.8047	2.5748	3/7 21:56	3/7 22:39	Night
227	40.8781	2.814	40.7962	2.8674	3/8 06:37	3/8 07:36	Sunrise
228	40.793	2.8705	40.758	2.929	3/8 07:39	3/8 08:12	Sunrise
229	40.7583	2.9361	40.8632	3.0378	3/8 08:16	3/8 09:26	Day
230	40.8693	3.0355	40.9432	2.9035	3/8 09:30	3/8 11:09	Day
231	40.9409	2.9019	40.9079	2.9165	3/8 11:21	3/8 11:42	Day
232	40.9068	2.9188	40.9565	2.9534	3/8 11:49	3/8 12:24	Day
233	40.9592	2.9566	41.0036	3.0643	3/8 12:26	3/8 13:20	Day
234	41.0064	3.0605	41.0466	2.9213	3/8 13:32	3/8 14:36	Day
235	41.0463	2.9224	40.9711	2.7884	3/8 14:35	3/8 15:53	Day
236	40.9663	2.7862	40.7335	2.7586	3/8 15:56	3/8 18:18	Sunset
237	40.7294	2.7598	40.6867	2.7842	3/8 18:21	3/8 18:50	Sunset

238	40.6849	2.78	40.7298	2.6792	3/8 18:55	3/8 19:51	Night
239	40.7341	2.6769	40.9679	2.6479	3/8 20:47	3/8 23:24	Night
240	40.9719	2.6455	40.9589	2.5418	3/9 00:30	3/9 01:13	Night
241	40.9538	2.5364	40.7413	2.4903	3/9 01:17:14	3/9 03:22:17	Night
242	40.7396	2.4868	40.7738	2.3611	3/9 03:25:18	3/9 04:34:53	Night
243	40.7779	2.3592	40.9475	2.4514	3/9 04:38:08	3/9 06:28:06	Sunrise
244	40.9517	2.4514	40.9725	2.435	3/9 06:30:51	3/9 06:45:16	Sunrise
245	40.9744	2.4283	40.8983	2.2367	3/9 06:49	3/9 08:29	Sunrise
247	40.9581	2.704	40.7797	2.725	3/9 10:38	3/9 12:26	Day
248	40.7748	2.7282	40.7759	2.7896	3/9 12:29	3/9 12:57	Day
249	40.7806	2.7977	41.0393	2.8693	3/9 13:02	3/9 16:25	Day
250	41.0462	2.8748	41.1015	2.9618	3/9 16:30	3/9 17:28	Sunset
251	41.0904	2.9486	40.8422	2.8395	3/9 19:28	3/9 23:28	Night
252	40.8405	2.8219	40.9518	2.3323	3/9 23:45	3/10 05:19	Night